

BRNO UNIVERSITY OF TECHNOLOGY
FACULTY OF CHEMISTRY

Assoc. Prof. Oldřich Zmeškal, Ph.D.

**USE OF THE FRACTAL THEORY TO STUDY PHYSICAL
AND CHEMICAL PROPERTIES OF MATERIALS**

**UŽITÍ TEORIE FRAKTÁLŮ PŘI STUDIU FYZIKÁLNĚ
CHEMICKÝCH VLASTNOSTÍ MATERIÁLŮ**

A THESIS OF A TALK FOR THE PROFESSORIAL APPOINTIVE
PROCEDURE IN THE STUDY FIELD OF
MATERIAL SCIENCE



BRNO 2005

Key words

Particle physics, physical fields of fractal structures, electrical and thermal properties of the fractal structures, theory of relativity of fractal structures

Klíčová slova

Fyzika elementárních částic, fyzikální pole fraktálních struktur, elektrické a tepelné vlastnosti fraktálních struktur, teorie relativity fraktálních struktur

© Oldřich Zmeškal, 2005

ISBN 80-214-2938-0

ISSN 1213-418X

Abstract

Focus of the work is the use of the fractal theory to study physical and chemical properties of materials. First part contains short introduction to fractal theory and definition of basic properties used to describe fractals (Fractal dimension D and Fractal measure K). Description of the fractal structures by common properties of substances and fields (like structure density, field intensity and field potential, density of the energy and flow of the field energy) and application of commonly known laws of physics in fractal like environment is main focus of the next part. The results of examination of physical laws in fractal like environment are more generalized by re-defining of those laws. New definition of laws describing gravitational and electrostatic interactions have been found as well as new definitions of laws describing expansion of the matter, electric charge and that of the heat (or energy in general) throughout the environment. The results were then defined also for non-inertial reference systems. The experiments to prove re-defined laws have been made by the author for two main areas of the research. First is related to the area of research of the space charge limited currents (SCLC) and defining distribution of densities of the energetic states of the semiconductors. The second experimental area is related to the distribution of heat in material and determining of material's heat related properties.

Abstrakt

Práce je zaměřena na použití teorie fraktálů při studiu fyzikálně-chemických vlastností materiálů. V první části je proveden stručný úvod do teorie fraktálů, jsou definovány základní parametry popisující vlastnosti fraktálních struktur (fraktální dimenze D a fraktální míra K). V další části jsou aplikovány veličiny popisující vlastnosti látek a polí (např. hustota struktury, intenzita a potenciál pole, hustota a tok energie pole) na různé druhy fraktálních struktur. Výsledkem jsou například zobecněné zákony popisující gravitační a elektrostatické interakce, zákony popisující šíření látky, elektrického náboje a tepla (obecně energie) prostředím. Výsledky jsou také zobecněny na pohybující se vztažné soustavy (teorie relativity). Dvě oblasti výzkumu jsou doplněny experimenty realizovanými autorem. První z nich se týká problematiky proudů omezených prostorovým nábojem (SCLC) a zjišťováním energetického rozdělení hustoty stavů v pohyblivostní mezeře polovodičů. Druhá z nich je zaměřena na studium šíření tepla látkovým prostředím a zjišťováním jeho tepelných parametrů.

Contents

1.	INTRODUCTION	6
2.	FRactal DIMENSION AND Fractal MEASURE.....	8
3.	FIELD AND POTENTIAL OF Fractal STRUCTURES.....	11
4.	ELECTROSTATIC AND GRAVITATIONAL FIELD.....	14
5.	UNIFYING INTERACTIONS BETWEEN PARTICLES.....	17
6.	Thermal FIELD.....	22
7.	STEADY STATE ELECTRIC CURRENT.....	32
8.	TIME DEPENDENCES OF Fractal QUANTITIES	37
9.	CONCLUSION.....	44
10.	REFERENCES.....	44

Author's introduction

Name: Assoc. Prof. Oldřich Zmeškal, Ph.D.

Date of birth: December 7, 1953 in Velké Meziříčí

Education and degrees:

Dipl. Eng. - Specialization: Computer Science (1978)

Faculty of Electrical Engineering, Military Academy, Brno

Thesis: "Use of Nonlinear Programming for Dynamic Processes in Thin Layer Systems in Amorphous Semiconductors"

Ph.D. - Specialization: Applied Physics (1983)

Faculty of Electrical Engineering, Military Academy, Brno

Thesis: "Transport of Charge in Heterostructures with Amorphous Semiconductors for Applications in Optoelectronics"

Assoc. Prof. - Specialization: Material Engineering (1994)

Faculty of Electrical Engineering, Military Academy, Brno

Thesis: "Methods of Study of the Space Charge in Amorphous Semiconductors "

Professional experience:

1978 - 1983 Research Institute of the Czechoslovak Army General Staff, Scientist

1979 - 1983 Department of Physics, Military Academy, Brno, Postgraduate Student

1984 - 1993 Department of Physics, Military Academy, Brno, Assistant Lectures

since 1993 Institute of Physical and Applied Chemistry, Faculty of Chemistry, Brno University of Technology, Assistant Professor, Associate Professor, Head of Institute of Physical and Applied Chemistry, Vice-dean for Education,

Research activities:

Modelling of transport phenomena in amorphous semiconductors. Temperature Modulated Space Charge Limited Currents (TM SCLC), Temperature Modulated Field Effect (TM FE), Meyer - Neldel rule in semiconductors. Kinetics of chemical processes in organic and inorganic materials. Image Science and Color Management

Publication activities:

Author or co-author

7 chapters in monographs, 10 study texts, 22 journal publications (17 internationals), 4 program products, 10 lectures and 20 posters on Czech and international conferences, 35 contributions in proceedings of Czech and international conferences, 9 special research reports. Supervisor of 18 diploma students, supervisor of 6 Ph. D. students

Teaching:

Basic lectures: Physics, Computer Science, Informatics and Fundamentals of Statistics, Fundamentals of Informatics, Fundamentals of Image Science

Ph.D. lectures: Mathematics, Computer Controlled Experiment, Information Technology in Chemistry

1. INTRODUCTION

Several geometrical shapes with “strange” properties have been first discovered in the end of the 19th century. The structure of the objects was resolution independent, i.e. the shape of the object was exact or approximate magnification of its part. One of the first objects described was for example Classic Cantor set (described by German mathematician George Cantor, 1845 – 1918). Classical Cantor set of the metric space is obtained by successive deletion of middle-third open subintervals in one dimensional metric space $[0, 1]$, see *Figure 1a*. This set is a perfect set that contains unaccountably many points. The other interesting objects discovered by that time were for example Koch curve and Peano curve. Swedish mathematician Niels Koch (1870 – 1924) created it by replacing basic line in metric space $[0, 1]$ by couple of minimized parts of the same size (4 lines of the size of $1/3$, see *Figure 1b*). Italian mathematician Giuseppe Peano (1858 – 1932) created it by replacing basic line in metric space $[0, 1]$ by 16 lines of the size of $1/4$ (see *Figure*

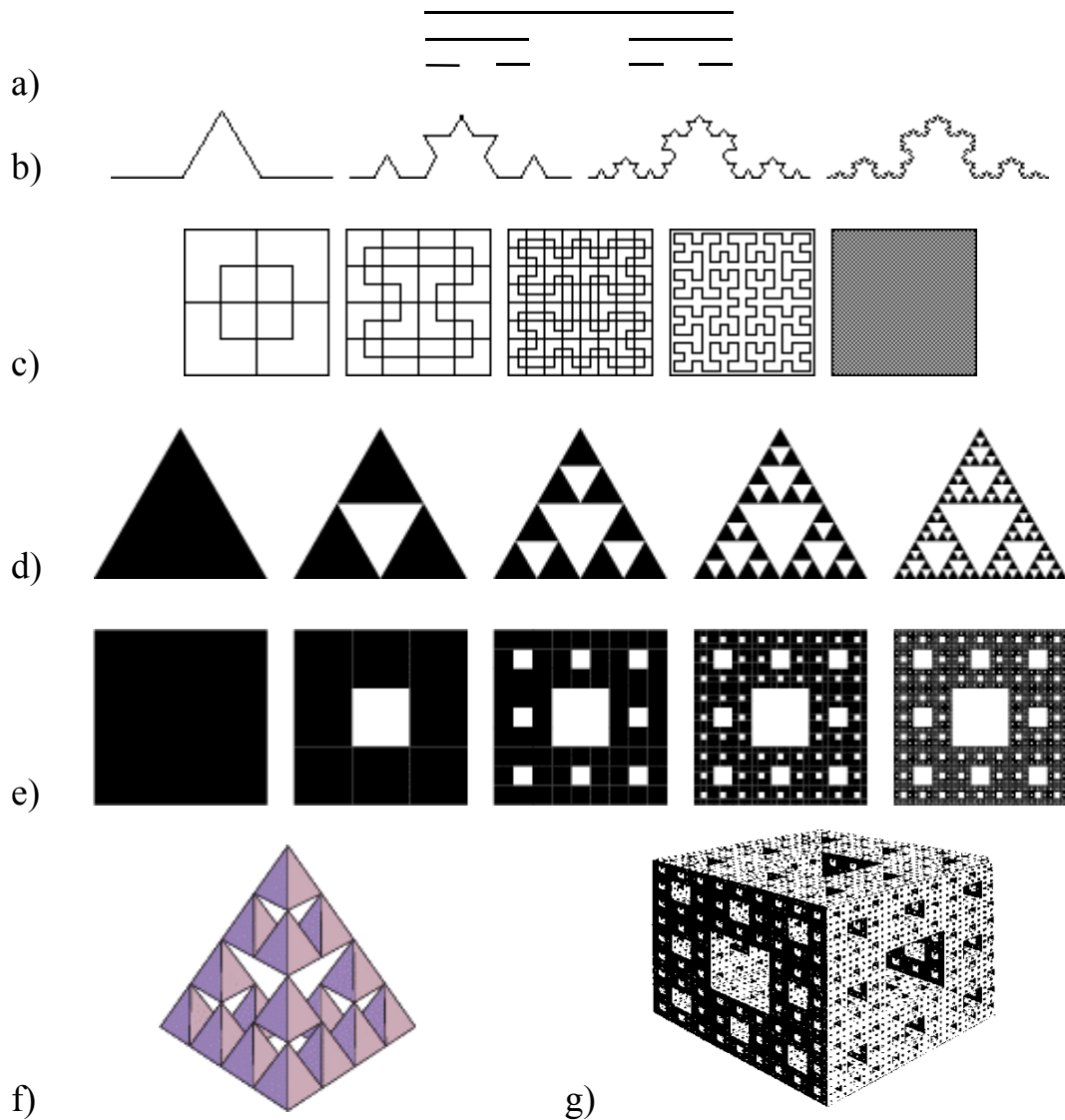
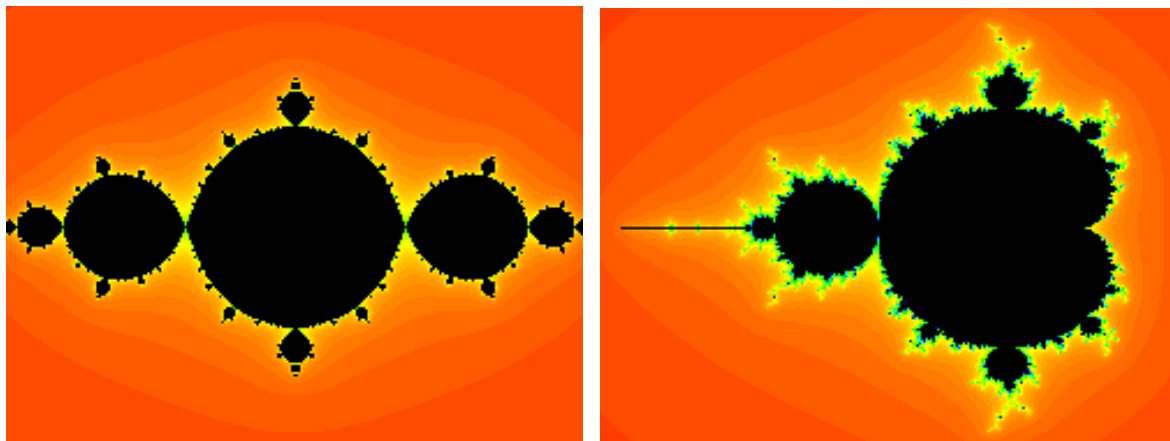


Figure 1 Examples of fractal structures in one-, two- and three-dimensional metric space a) Cantor discontinue, b) Koch curve, c) Peano curve, d) Sierpinsky triangle, e) Sierpinsky carpet, f) Sierpinsky tetris and g) Sierpinsky sponge

1c). Obtained curves shows very interesting properties after infinite number of iterations. They are continuous in all of their points, are infinite (Peano curve would also fill completely two-dimensional space). Nice example of the removal of the minimized areas of object is Sierpinsky triangle or Sierpinsky carpet (polish mathematician Waclaw Sierpiński, 1882 – 1969), see *Figure 1d* and *Figure 1e*. Objects created by that way contain uncountably many points in the infinitely small area enclosed by infinitely long curve. Analogically the three dimensional objects can be constructed (like Sierpinsky tetris and Sierpinsky sponge, see *Figure 1f* and *Figure 1g*). Huge surface area and very small volume are typical properties of such objects. The structures described above are commonly called **linear deterministic fractals**.



a) *Figure 2 a) Julia set $f(z) = z^2 - 1$ and b) Mandelbrot set $f_\lambda(z) = z^2 - \lambda$ (black regions) and their around, displayed with colour grades (on the figure are evident individual analytic curves, separated by different levels)*

Another known way to construct fractal objects is represented by Julia–Fatou set (French mathematician Pierre Fatou, 1878 – 1929, French mathematician Gaston Julia, 1893 – 1978). The set is defined by $f(z) = z^2 - 1$, see *Figure 2a*. The constructing function was obtained as a result of the study of iterations of *rational fractional functions in the complex number set* with different values of initial properties. Use of the defining function has grown on importance when it became possible to perform iterative calculations using computers in second half of the last century. The main research on fractals at the time was done by French mathematician Benoit Mandelbrot (1924). Mandelbrot published results of his work in the book *The fractal geometry of nature* in 1982 [1]. Often used example of his work is so called Mandelbrot set defined as $f_\lambda(z) = z^2 - \lambda$ in the plane of the complex variable λ (constructed for $z = (0,0)$), see *Figure 2b*. This type of fractals is also called **nonlinear deterministic fractals**.

It has been found that a lot of natural structures and objects has fractal characteristic in the first half of last century. Typical example of such structures used often in literature is the measured coastal length in dependency on the scale of the map used. It is obvious that the length of curve marking the shape of the coast grows with the scale of the map used. One of the scientists who helped with the research of self-similar structures was British mathematician Lewis Richardson (1881 – 1953). Richardson collected big amount of the empirical data related to the measurement of the length of the different coastlines and of the length of rivers (*Figure 3*). He presented results of the measurement in logarithmic graph as dependency of the length on the scale $\log L(\varepsilon) = f(\log(\varepsilon))$.

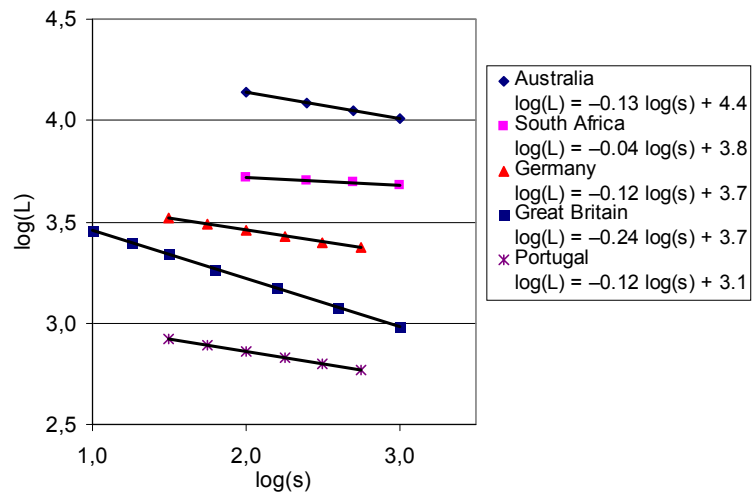


Figure 3 Coastal length in relation to the scale of the map for different countries and continents (in text $s = \varepsilon$).

Richardson collected big amount of the empirical data related to the measurement of the length of the different coastlines and of the length of rivers (*Figure 3*). He presented results of the measurement in logarithmic graph as dependency of the length on the scale $\log L(\varepsilon) = f(\log(\varepsilon))$. Based on his own experience in mathematics Robertson derived the empiric equation for describing the length of the coast on the scale used as

$$L(\varepsilon) = K \cdot \varepsilon^{1-D} \quad (1.1)$$

where ε is the length of stick used for measurement, $L(\varepsilon)$ the total length of the coast, K and D are the constants for the coast measured (see *Figure 3*). Mandelbrot published posthumously the results of his work in 1961. Richardson's empiric equation for coastal length written as

$$K = N(\varepsilon)\varepsilon^D \quad (1.2)$$

where $N(\varepsilon) = L(\varepsilon) \cdot \varepsilon^{-1}$ is amount of distances of the length ε , reminded him the equation for Hausdorff–Besicovitch measure (German mathematician Felix Hausdorff, 1868 – 1942, Russian mathematician Abram Besicowitch, 1891 – 1970).

Benoit Mandelbrot has described fractals by a mathematical apparatus, which makes it possible to determine their two characteristic parameters (the Hausdorff – Besicovitch outer measure K and the Hausdorff – Besicovitch dimension D) [1].

2. FRACTAL DIMENSION AND FRACTAL MEASURE

The definition of fractal dimension is based on Hausdorff's d -dimensional outer measure H^d , which is defined as a subset of the n -dimensional Euclidean space E_n ($n = 0, 1, 2, \dots$) [1]

$$H^d = \liminf_{\varepsilon \rightarrow 0} \inf_M \left[\sum_{A \in M} (\text{diam } A)^d \right], \quad (2.1)$$

where $\sum_{A \in M} (\text{diam } A)^d$ means covering of space E_n by set A . Each of $A \in M$ has diameter smaller than ε ($\varepsilon > 0$, $\text{diam } A < \varepsilon$).

Hausdorff's measure as a function of parameter d ($d \geq 0$) is not a growing function and its possible values are from interval $\langle 0, \infty \rangle$

- if for any $\delta > 0$ $H^\delta < \infty$ exists, then for all $d > \delta$ $H^d = 0$,
- if for any $\delta > 0$ $H^\delta > 0$, then for all $d \in \langle 0, \delta \rangle$ $\lim_{\varepsilon \rightarrow 0} H^d(E) \rightarrow \infty$.

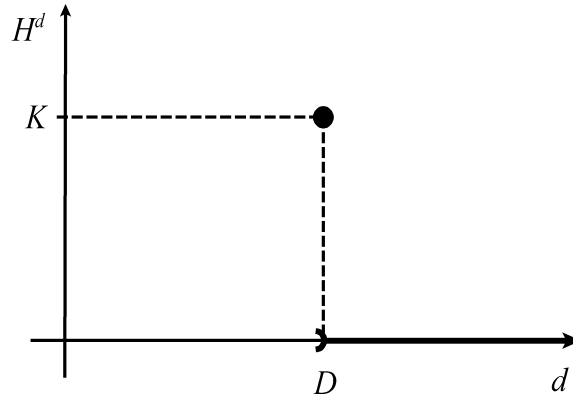


Figure 4 Hausdorff's d -dimensional external measure, D – Hausdorff – Besicovitch (fractal) dimension, K – Hausdorff – Besicovitch (fractal) measure

The result of previous conditions is that there exists just one constant D for parameter d , when the Hausdorff's measure is equal to the non-zero finiteness value $H^d = K$. This constant is called Hausdorff – Besicovitch outer measure (Figure 4). By covering n -dimensional space E_n with objects of m -dimensional space E_m ($E_m \subseteq E_n$, $m \leq n$), we can assume Hausdorff - Besicovitch dimension values $D \in \langle m, n \rangle$. If the objects of the covering are the same

$$\inf_M \left[\sum_{A \in M} (\text{diam } A)^d \right] = N(\varepsilon) \cdot \varepsilon^d \quad (2.2)$$

then it is possible to write the Hausdorff's measure in the form

$$H^d = \lim_{\varepsilon \rightarrow 0} N(\varepsilon) \cdot \varepsilon^d \quad (2.3)$$

where $N(\varepsilon)$ is the amount of covering of size ε . Due to this condition, Hausdorff's outer measure ($0 < H^d < \infty$) is usually labelled as a fractal measure (K) and Hausdorff - Besicovitch dimension as a fractal dimension (D).

Fractal measure K of these objects can be expressed using Eq. (2.3)

$$K = N(\varepsilon)\varepsilon^D \quad (2.4)$$

and fractal dimension is given by the slope of function (2.4)

$$D = - \frac{d \ln N(\varepsilon)}{d \ln \varepsilon} \quad (2.5)$$

where m is the number of repetitions of the reduced fractal pattern of size r_0 and $1/r$ is the ratio of its reduction.

Fractal dimension of 2D objects (the plane) can be determined numerically using the equations above with the help of computers by the “*box counting method*” or by the “*mass method*”, [2], [3]. Both methods are complementary ($\varepsilon = 1/r$) and produce the same values of fractal dimension D . Therefore taking the real situations into consideration; we will use evaluations with r . The area filled by the examined set (points) can be expressed as:

$$S(r) = \frac{N(r)}{r^2} = K \cdot r^{D-2} \quad (2.6)$$

Eq. (2.6) can be transformed into (2.7) for the general Euclidean space E_n (we will denote its dimension as $E = n$)

$$F(r) = \frac{N(r)}{r^E} = K \cdot r^{D-E} \quad (2.7)$$

The value of $F(r)$ will be called as *coverage of space*. The last equation implies that fullness of space depends on its size (determined, e.g., by the length of the edge r of E -dimensional space) and also on the parameters K and D .

Fractal dimension can vary in the interval $D \in \langle 0, E \rangle$, where $E = n$. In limit cases:

- The mean value of density of quantity for $D = 0$ (e.g. there is a constant number of objects independent of the size of space, $N(r) = K$) decreases according to the equation $F(r) = K \cdot r^{-E}$ (for $r > 1$).
- The coverage of space is independent of the space size for $D = E$ (e.g., the space is homogeneously filled) and is equal to the fractal measure $F(r) = K$. The number of objects in the circumscribed area (for $r > 1$) increases with its size $N(r) = K \cdot r^E$.

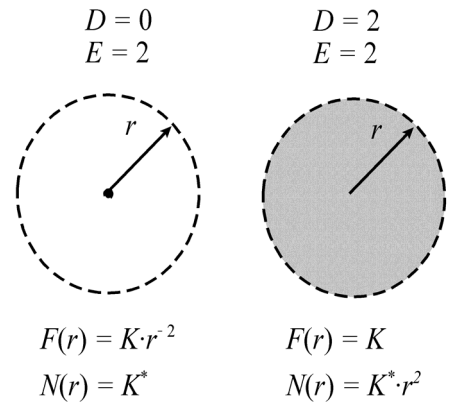


Figure 5 The coverage of two-dimensional space

The situation for 2D space is represented in Figure 5; different constants K and K^* are related to radial demarcation of space (the square demarcation in the box counting was replaced with the circle demarcation).

3. FIELD AND POTENTIAL OF FRACTAL STRUCTURES

In the next part, we will use this purely mathematical apparatus for the description of a physical field. The field will represent a set whose properties we study, as we have performed mathematically. As an example of application of the mathematical apparatus mentioned in previous chapters, we can use the distribution of physical quantity $Q(r)$ and density of physical quantity $\rho(r)$ in the E -dimensional space.

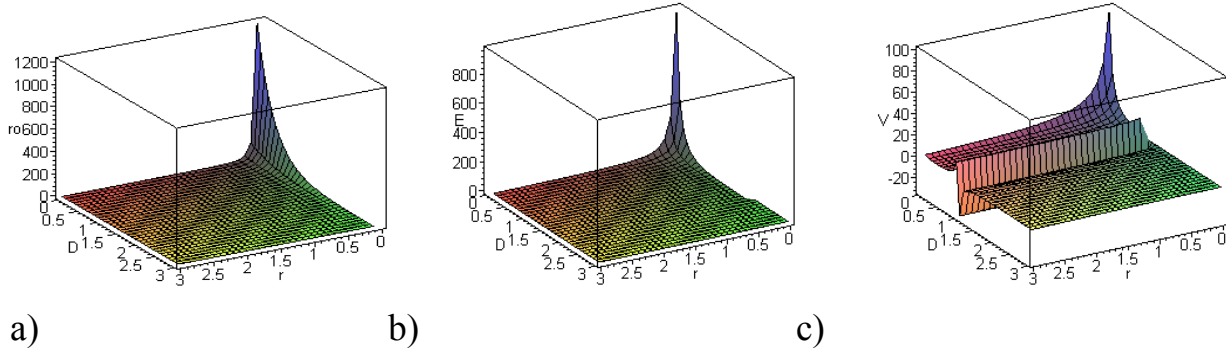


Figure 6 The dependences of physical quantities on the distance r and fractal dimension D a) radial density of physical quantity $\rho(r, D)$, b) radial part of the intensity of field $E_r(r, D)$ and c) radial part of the potential of physical field $V_r(r, D)$ for topological dimension $E = 3$

The mean value of density of physical quantity in the cell can be determined as the ratio of the quantity and the cell volume

$$\rho(r) = eF(r) = eK \cdot r^{D-E} \quad (3.1)$$

We will calculate the physical quantity $Q(r)$ (e.g. mass or electric charge) in contrast to [4] by equation

$$Q(r) = \int_{V^*} \rho dV^* = eK \frac{E r^D}{D} = \frac{E r^E}{D} \rho(r) \quad (3.2)$$

where $dV^* = d(r^E)$ is an elementary volume of E -dimensional space.

This quantity is (see Eq. (2.7)) related to the coverage of the space. It is evident that the density of the quantity depends on the fractal dimension D , on the fractal measure K and on its distribution in the E -dimensional space. This distribution is expressed by Figure 6a (in appropriate units). It turns out that for the fully covered space ($D = E$) the distribution of the physical quantity is homogenous in the space. For the space where just one elementary cell is placed the charge density of in the cell of size r is given by $\rho(r) = 1/r^E$ (with the growing size of the cell, the coverage of space decreases).

The change in the mean value of density $\rho(r)$ of physical field with the change of size r by dr can be determined by the Gauss-Ostrogradsky law

$$\text{div } \mathbf{E} = k \cdot \rho(r) \quad (3.3)$$

The vector \mathbf{E} defines the intensity of physical field of scalar $\rho(r)$. The radial component of intensity E_r (when field is point-symmetric), can be written

$$\frac{D}{D-E+1} \frac{dE_r}{dr} = k \cdot \rho(r) \quad (3.4)$$

By integration of Eq. (3.4), we obtain for radial distribution of physical field intensity equations

$$E_r = eK^* \frac{D-E+1}{D} \int r^{D-E} dr = eK^* \frac{r^{D-E+1}}{D} \quad (3.5)$$

Figure 6b shows dependency of the radial component of a physical field for different values of fractal dimension. The intensity is decreasing for $D < E - 1$ and increasing for $D > E - 1$, for $D = E - 1$ it is constant (homogenous field).

The physical field \mathbf{E} and the potential V are related as follows

$$\mathbf{E} = -\text{grad} V, \quad (3.6)$$

so both quantities are determined by a density $\rho(r)$ distribution

$$\Delta V = -\text{div} \mathbf{E} = -k \cdot \rho(r), \quad (3.7)$$

where Δ is so-called Laplace operator.

This equation can be written for the radial distribution of a physical field's density $\rho(r)$ as

$$\frac{D}{D-E+1} \frac{d^2 V_r}{dr^2} = -k \cdot \rho(r) \quad (3.8)$$

From Eq. (3.7) we can determine the corresponding dependence of the potential of physical field

$$V_r = -eK^* \frac{r^{D-E+2}}{D(D-E+2)} \quad (3.9)$$

The dependence of the potential of physical field radial part for different values of fractal dimension is presented on Figure 6c. The potential is positive for $D < E - 2$ and negative for $D > E - 2$. The potential is constant For $D = E - 2$ (in special case equal to zero: intensity of field is constant – homogenous field).

Four limit cases are discussed in next part ($D = 0$, $D = E - 2$, $D = E - 1$, $D = E$)

- For an "empty" space (the physical quantity is of point character, $Q = \text{const.}$), when $D = 0$, the intensity and potential depend on the cell size by term

$$E_r = kE \frac{Q}{r^{E-1}}, \quad V_r = -\frac{kE}{E-2} \cdot \frac{Q}{r^{E-2}} \quad (3.10)$$

- For the fully covered space when $D = E$ (the density of a physical quantity does not depend on the space size, $\rho = \text{const.}$), the intensity of a physical field increases linearly and the potential increases parabolic with the size of cell which bounds the E -dimensional space

$$E_r = \frac{k\rho}{E} r, \quad V_r = -\frac{k\rho}{2E} r^2. \quad (3.11)$$

- The case when $D = E - 1$ corresponds to second boundary, when the field intensity is constant (homogenous field), the potential linearly increases consequently. If we express the volumetric charge density by the relation $\rho = eK/r = \sigma/r$, where $\sigma = \text{const.}$ is surface charge density, we obtain

$$E_r = \frac{k\sigma}{E-1} = \text{const.}, \quad V_r = -\frac{k\sigma}{E-1} r. \quad (3.12)$$

- The case when $D = E - 2$ corresponds to the boundary, when the potential is constant. If we express volumetric charge density by the equation $\rho = eK/r^2 = \tau/r^2$, where $\tau = \text{const.}$ is linear charge density, we obtain

$$E_r = \frac{k\tau}{(E-2)r}, \quad V_r \approx -\frac{k\tau}{(E-2) \cdot 0} \rightarrow \infty. \quad (3.13)$$

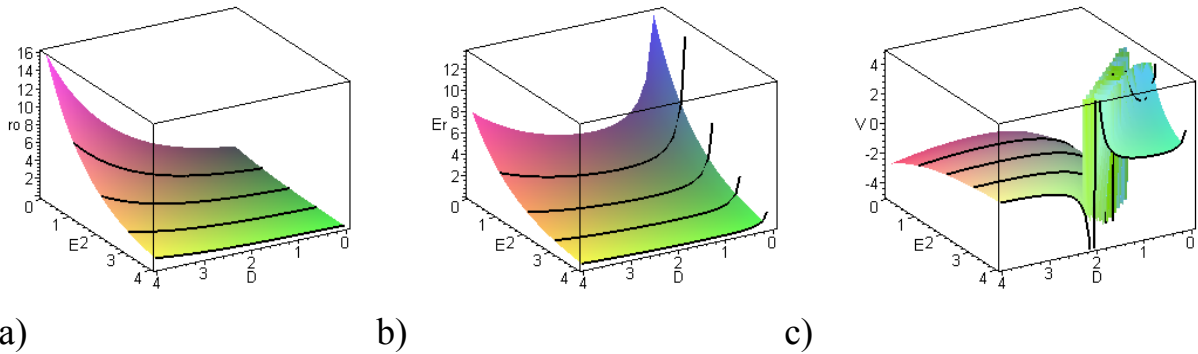


Figure 7 The dependences of physical quantities on the topological E and fractal dimension D a) radial density of physical quantity $\rho(r, D)$, b) radial part of the intensity of field $E_r(r, D)$ and c) radial part of the potential of physical field $V_r(r, D)$ for distance $r = 2$

Figure 7b gives the radial intensity of a physical field versus fractal dimension dependence. It is derived from Figure 6b by cuts for different values of $r = \text{const.}$). The parameter of this dependence is the cell size r . The figure demonstrates that the values of field intensity are decreasing for lower values of bounded space radius and increasing for its higher values (for the same density of quantity in $r = 1$), see Figure 6. Intensity of field is independent on bounded area radius for $D = E - 1$. This case is called as homogenous field.

In Figure 7c the radial potential of a physical field versus fractal dimension dependence is outlined. It is derived from Figure 6c by cuts for different values of $r = \text{const.}$). The parameter of this dependence is the cell size r . The figure

demonstrates that the values of field potential are positive for fractal dimension $D \in (0, E - 2)$, negative for $D \in (E - 2, E)$ and for $D = E - 2$ they are constant (they do not depend on the size of bounded area), for $D = 0$ they are multiplied by $1/r$ coefficient.

In praxis the dependencies of potential on intensity are often measured. From the Eq. (3.5) and (3.9) this dependency can be expressed by the Eq. (3.14)

$$E_r = -(D - E + 2)V_r/r \quad (3.14)$$

From the density of quantity (3.1), from intensity of field (3.5) and from potential of physical field (3.9) the following parameters can be derived:
the differential specific capacity of physical field

$$c = \frac{\rho}{V_r} = -\frac{D(D - E + 2)}{k r^2}, \quad (3.15)$$

the density of energy

$$w = \rho V_r = -c V_r^2 = -\frac{D(D - E + 2)}{k} \left(\frac{V_r}{r} \right)^2 \quad (3.16)$$

and the flow of energy

$$i = \rho E_r = \frac{k}{D} \rho^2 r = \frac{D}{kr} E_r^2 \quad (3.17)$$

These terms are independent on the margin conditions.

4. ELECTROSTATIC AND GRAVITATIONAL FIELD

Fractal dimension can vary between two limits:

- for $D = 0$ the change of structure of fractal as the function of size of measure will be maximum (in the real world e.g. the idealised objects mass point or point charge represent such situation),
- for $D = E$, where E is Euclidean dimension the change of fractal structure will not depend on the change of measure (in the real world e.g. the idealised object rigid body represents this situation).

The density of this quantity $\rho(r)$ (e.g. density of mass or electric charge) for 3D Euclidean space ($E = 3$) can be written as (Eq. (3.1))

$$\rho(r) = \rho_0 r^{D-3}, \quad (4.1)$$

where e is the size of the elementary quantity, $\rho_0 = eK$.

We will calculate the physical quantity $Q(r)$ (e.g. mass or electric charge, Eq. (3.2)) by equation

$$Q(r) = \rho_0 \frac{3r^D}{D} = Q_0 r^D, \quad (4.2)$$

where $dV^* = d(r^E)$ is an elementary volume of E -dimensional space and $Q_0 = 3\rho_0/D$ is the electric charge for sphere with radius $r = 1$.

$$E_r = k\rho_0 \cdot \frac{r^{D-2}}{D}, \quad V_r = -k\rho_0 \cdot \frac{r^{D-1}}{D(D-1)}. \quad (4.3)$$

Constant k has different values for different type of field and fractal dimension (see *Table I*).

Table I. Notable fractal dimension in E - dimensional space

D	independent quantity	type of field	volume	$k\rho_0$	$k\rho_0$
0	$Q = \text{const.},$ $M = \text{const.}$	point quantity/spherical	$V^* = 4\pi r^3/3$	$Q_0/4\pi\epsilon_0$	GM_0
$E - 2$	$V_r = \text{const.}$	equipotential/cylindrical	$V^* = 2\pi r^3$	$\tau_0/2\pi\epsilon_0$	$2G\tau_0$
$E - 1$	$E_r = \text{const.}$	homogenous intensity/plane parallel	$V^* = 8r^3$	σ_0/ϵ_0	$4\pi G\sigma_0$
E	$\rho = \text{const.}$	homogenous density		ρ_0/ϵ_0	$4\pi G\rho_0$

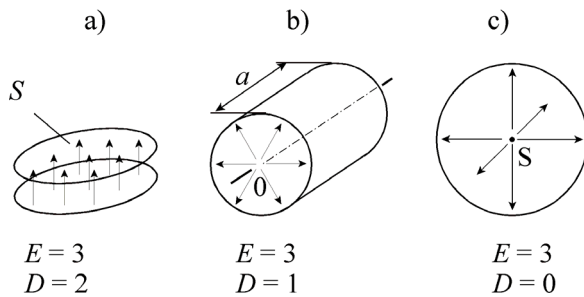


Figure 8 Special geometry for a) plane-parallel, b) cylindrical and c) spherical coordinates Euclidean space

homogenously charged thin pole ($D = E - 2 = 1$), respectively. The relations describing electrostatic field in the surroundings of point charge ($D = 0$) and the electrostatic field inside homogenously charged body ($D = E = 3$) are presented too (see *Figure 8*).

- For dimension of Euclidean space $E = 3$ and fractal dimension $D = 0$, e.g. the electric intensity E_r and potential V_r at the distance r from the point electric charge Q (the minus sign is included in the electric charge in this case $Q < 0$) can be the *Eq. (3.10)* expressed as

The values defined in the previous part are used for the description of the properties of electrostatic field with the defined distribution of electric charge. There are some special cases, which will be discussed in following – e.g. intensity and potential (*Eq. (3.5)* and (*3.9*)) of field around uniformly charged surface ($D = E - 1 = 2$) and

$$E_r = \frac{1}{4\pi\epsilon_0\epsilon_r} \cdot \frac{Q}{r^2}, \quad V_r = -\frac{1}{4\pi\epsilon_0\epsilon_r} \cdot \frac{Q}{r}, \quad (4.4)$$

where $\epsilon_0\epsilon_r$ is the permittivity of the environment, and $k = 3/(4\pi\epsilon_0\epsilon_r)$ and $4\pi/3$ is the coefficient for transformation from cube to sphere space.

- In 3D space ($E = 3$) the situation on Eq. (3.11) (for $D = E$) is represented e.g. by the electric field potential inside a homogeneously charged space, with the constant volumetric charge density ρ

$$E_r = \frac{\rho}{3\epsilon_0\epsilon_r} r, \quad V_r = -\frac{\rho}{6\epsilon_0\epsilon_r} r^2, \quad (4.5)$$

where $k = 1/\epsilon_0\epsilon_r$.

- In 3D space ($E = 3$) the situation on Eq. (3.12) represents e.g. the electrical fields intensity and potential around a uniformly charged surface ($D = E - 1 = 2$) with the constant surface charge density σ

$$E_r = \frac{\sigma}{2\epsilon_0\epsilon_r} = \text{const.}, \quad V_r = -\frac{\sigma r}{2\epsilon_0\epsilon_r}, \quad (4.6)$$

where $k = 1/\epsilon_0\epsilon_r$.

- In 3D space ($E = 3$) the situation on Eq. (3.13) represents e.g. the electrical fields intensity and potential around a non-conductive, homogeneously charged pole ($D = E - 2 = 1$) with the constant linear charge density τ .

$$E_r = \frac{\tau}{2\pi\epsilon_0\epsilon_r r}, \quad V_r = \frac{\tau \ln(r/r_0)}{2\pi\epsilon_0\epsilon_r}, \quad (4.7)$$

where $k = 1/2\pi\epsilon_0\epsilon_r$, π is the coefficient for transformation from cube to cylinder space and r_0 is distance of the pole from position of zero potential ($r_0 \rightarrow \infty$).

By the integration of differential specific capacity of physical field over volume dV^* (3.15) it can be derived the capacity of fractal matter in the space of volume $V^* = r^E$

$$C(r) = \int_{V^*} c dV^* = \frac{ED(D - E + 2)}{k(E - 2)} r^{E-2} = \frac{D}{E - 2} \cdot \frac{Q}{V_r}. \quad (4.8)$$

Using this quantity it is possible to define e.g. electrical capacity of homogeneously charged planar board of size S ($D = 2, E = 3$) at distance r

$$C = 2 \frac{Q}{V_r} = \frac{2\epsilon_0\epsilon_r S}{r}, \quad (4.9)$$

where $Q = \sigma S/2$ (4.2) is a charge on the planar board and $V_r = \sigma r/2\epsilon_0\epsilon_r$ (4.6) is a potential at a distance r from this. As generally known, the capacity of planar capacitor (two planes at distance r) is half.

By the integration of density of energy of physical field (3.16) over the volume dV^* we can determine the energy of fractal object in the space of size (volume) $V^* = r^E$

$$E(r) = \int_{V^*} w dV^* = \frac{k(eK)^2 E}{D(D-E+2)(2D-E+2)} r^{2D-E+2} = -\frac{D}{2D-E+2} QV_r \quad (4.10)$$

and the force among these fractal objects

$$F(r) = -\text{grad } E(r) = -\frac{k(eK)^2 E}{D(D-E+2)} r^{2D-E+1} = -\frac{D}{D-E+2} QE_r \quad (4.11)$$

5. UNIFYING INTERACTIONS BETWEEN PARTICLES

Links between inverse coupling constants of various interactions (gravitational $\bar{\alpha}_G \approx 10^{38}$, weak $\bar{\alpha}_W \approx 10^5 - 10^8$, electromagnetic $\bar{\alpha}_{EM} \approx 137$ and strong $\bar{\alpha}_S \approx 0.1 - 10$) in the three-dimensional Euclidean space are discussed.

The analysis is based on the fact that such interactions between particles are generally realised both, by photons (electromagnetic radiation) and by particles. Ideal limit cases arise for $\bar{\alpha} \rightarrow \infty$ (the interaction is mediated just by photons) and for $\bar{\alpha} = 0$ (completely mediated by particles).

Current theories of elementary particles are associated with certain ‘groups’, which obey the mathematics of group theory [8], [9]:

- The electromagnetic (QED) group U(1) has one gauge boson (the photon).
- The electroweak (QED) group SU(2) has 3 gauge bosons (W^+ , W^- and Z bosons)
- The strong (QCD) group SU(3) has 3 gauge and 5 Higgs bosons (H^+ , H^- , H^0 , \bar{H}^0 and A^0 bosons)

The simplest GUT is labelled SU(5) and has 24 bosons. We have already 8 (gauge and Higgs bosons). There would also be 8 bosons (leptoquarks Y and X) with three different colours (Y_R, Y_G, Y_B, Y_{RGB}), (X_R, X_G, X_B, X_{RGB}), plus their 8 anti-particles. These X and Y bosons can change quarks into leptons. This adds up to $(3)(8) = 24$ as should be.

Gravitational interactions are responsible for interactions between arbitrary mass particles. Using the equations above can **the gravitational inverse coupling constant** $\bar{\alpha}_G$ (e.g. interaction between two protons) be expressed as [8], [9]

$$\bar{\alpha}_G = \left(\frac{m_G}{m_p} \right)^2 = \frac{4\pi\epsilon_0\hbar c}{g_G^2} = \frac{\hbar c}{G_N} \cdot \frac{1}{m_p^2}, \quad (5.1)$$

where $m_G = m_{\text{Planck}} = \sqrt{\hbar c / G_N}$ is the mass constant of gravitational interaction (Planck's mass), $g_G = m_p \sqrt{4\pi\epsilon_0 G_N}$ is “the gravitational charge” in coulomb, \hbar is the modified Planck's constant, c is the speed of light and G_N is the Newton's gravitational constant (see *Table II*).

Table II. Interaction constants for protons

interaction	interaction constant	mass constant of interaction m_0	charge of interaction g_0 (C)	coupling constant for two protons
Gravitational G_N	$6.67259 \cdot 10^{-11} \text{ kg}^{-1} \cdot \text{s}^{-2} \cdot \text{m}^3$	$2.17671 \cdot 10^{-8} \text{ kg}$ $1.2227 \cdot 10^{22} \text{ MeV}$	$1.44120 \cdot 10^{-37}$	$1.69358 \cdot 10^{38}$
Weak G_F	$1.43587 \cdot 10^{-62} \text{ J} \cdot \text{m}^3$	$1.85034 \cdot 10^{-24} \text{ kg}$ $1.0394 \cdot 10^6 \text{ MeV}$	$1.69541 \cdot 10^{-21}$	$1.22379 \cdot 10^6$
Electromagnetic G_{EM}	$8.24644 \cdot 10^{25} \text{ kg}^{-1} \cdot \text{s}^{-2} \cdot \text{m}^3$	$1.95801 \cdot 10^{-26} \text{ kg}$ $1.0999 \cdot 10^4 \text{ MeV}$	$1.60218 \cdot 10^{-19}$	137.03599
Strong G_S	$1.97473 \cdot 10^{27} \text{ kg}^{-1} \cdot \text{s}^{-2} \cdot \text{m}^3$	$4.00124 \cdot 10^{-27} \text{ kg}$ $2.2476 \cdot 10^3 \text{ MeV}$	$7.84028 \cdot 10^{-19}$	5.7227

Weak interactions are responsible for: a) the continuous spectra of electrons emitted in the decay of radioactive nuclei, b) hadrons decays, c) all the reactions induced by neutrinos. **The weak inverse coupling constant** $\bar{\alpha}_W$ of a long-range interaction ($l > 10^{-15}$ m) (e.g. between two protons) can be explained as the exchange of neutrinos between them (Fermi's theory of weak interactions - 1930s) [9]

$$\bar{\alpha}_W = \left(\frac{m_W}{m_p} \right)^2 = \frac{4\pi\epsilon_0 \hbar c}{g_W^2} = \frac{4\pi \hbar^3}{c G_F} \cdot \frac{1}{m_p^2}, \quad (5.2)$$

where $m_W = (\hbar/c) \sqrt{4\pi \hbar c / G_F}$ is the mass constant of a weak interaction (Fermi's mass), $g_W = (m_p c / \hbar) \sqrt{\epsilon_0 G_F}$ is “the weak charge” in coulomb, \hbar is modified Planck's constant, c is the speed of light and G_F is the Fermi's coupling constant (see *Table II*).

Particles with non-zero electrical charge, which affect each other, constitute the electromagnetic interaction. **The electromagnetic inverse coupling constant** $\bar{\alpha}_{EM}$ of interactions between two charged particles (e.g. protons) can be defined as the rate of energy of electromagnetic interaction between two particles with elementary charge at distance equal to the Compton wavelength λ_C to the energy of the photon $E = m_f c^2 = \hbar c / \lambda_C$, where \hbar is Planck's constant and c is the speed of light [5]

$$\bar{\alpha}_{EM} = \left(\frac{m_{EM}}{m_p} \right)^2 = \frac{4\pi\epsilon_0\hbar c}{e^2} = \frac{\hbar c}{G_{EM}} \cdot \frac{1}{m_p^2}, \quad (5.3)$$

where $m_{EM} = \sqrt{\hbar c / G_{EM}}$ is the mass constant of electromagnetic interaction (Compton's mass), \hbar is modified Planck's constant, c is the speed of light, e is the elementary (electric) charge, m_p mass of proton and G_{EM} is the electromagnetic constant (see *Table II*). The inverse coupling constant is frequently called as the electromagnetic (Sommerfeld) fine structure constant.

As Maxwell unified electricity and magnetism into electromagnetism, Glashow, Weinberg and Salam (in 1970) showed that the electromagnetism and the weak interaction could be treated as different aspects of one 'electroweak' interaction.

The mass of a particle for which is the electromagnetic and weak interaction equal can be determined from the comparison of *Eq. (5.2)* and *(5.3)*

$$m_y = \frac{e\hbar}{c\sqrt{\epsilon_0 G_F}}. \quad (5.4)$$

The value $m_y \approx 1.58 \cdot 10^{-25}$ kg (≈ 88.7 GeV) indicates that the searched particle could be W boson [9], [10].

Strong interactions arise from short-range particle interactions (e.g. into a nucleus). These interactions are mediated by pions. **The strong inverse coupling constant** $\bar{\alpha}_S$ of interaction between two particles (e.g. protons) can be formally defined as the previous were

$$\bar{\alpha}_S = \left(\frac{m_S}{m_p} \right)^2 = \frac{4\pi\epsilon_0\hbar c}{g_S^2} = \frac{\hbar c}{G_S} \cdot \frac{1}{m_p^2}, \quad (5.5)$$

where $m_S = \sqrt{\hbar c / G_S}$ is the mass constant of strong interaction, \hbar is modified Planck's constant, c is the speed of light, $g_S = (m_p c / \hbar) \sqrt{\epsilon_0 G_S}$ is "the strong charge" in coulombs and G_S is the strong interaction constant (see *Table II*). The knowledge that the interaction is mediated by the exchange of pions between protons (nucleons) of a nucleus was used when the strong interaction constant was calculated.

It is obvious from *Table II* that the possible values of coupling constants of these basic interactions are from broad interval. An interaction can be described by two constants, by the charge of the interaction $g_0 = \sqrt{4\pi\epsilon_0\hbar c / \bar{\alpha}}$ (it is equal to the elementary charge for electromagnetic interaction between two protons) and by the mass constant of interaction m_0 (it is equal to Plank's constant for gravitational interactions). The mass of particles in interaction is directly proportional to their

product $m_y = m_0/\sqrt{\bar{\alpha}} = m_0 g_0/\sqrt{4\pi\epsilon_0\hbar c}$. Constants of other interactions are also mentioned in the table. The Fermi's coupling constant, which has a different physical meaning than the others, is presented for the weak interaction. There are also formally derived constants for electromagnetic and strong interactions, which correspond to the Newton's gravitational constant.

The electromagnetic coupling constant α_{EM} and the gravitational coupling constant α_G **increases** with energy while the strong coupling constant α_S and the weak coupling constant α_W **decreases**. This results from the fact that gravitation and electromagnetism has non-limited range, while the range of strong and weak interaction is much shorter.

An inverse coupling constant (electromagnetic, strong, week, etc.) is usually used to describe the interactions between high-energy particles. It is defined as a ratio between the relativistic mass of an equipotential field structure in E -dimensional space ($D = E - 2$, see *Table I*) and the relativistic mass of a particle with any other fractal dimension. From equation (4.10) we can derive

$$\bar{\alpha} = \frac{Q(r)V_r}{E(r)} = \frac{E - 2D - 2}{D} \quad (5.6)$$

Eq. (5.7) shows that the inverse coupling constant is generally defined as the ratio of the energy E_f (or mass m_f) of field of photon and the energy E_x (or mass m_x) of a particle which participate in the interaction

$$\bar{\alpha} = \frac{E_f}{E_x} = \frac{m_f}{m_x}, \quad (5.7)$$

where $E_f = m_f c^2 = Q(r)V_r$ and $E_x = m_x c^2 = E(r)$. As a result of this interaction, a new particle with energy E_y (or mass m_y , $m_y \geq m_x$ respectively) is produced

$$E_y = E_x + E_f, \quad m_y = m_x + m_f \quad (5.8)$$

In this case the inverse coupling constant $\bar{\alpha}$ can be expressed as

$$\bar{\alpha} = \frac{m_y - m_x}{m_x} \quad (5.9)$$

For the different mass of particles (and/or photons), which participate on the interaction, increases the coupling constant $\bar{\alpha}$ values in the interval $\bar{\alpha} \in \langle 0, \infty \rangle$.

Three limiting cases are discussed in what follows (see *Figure 9*):

- An interaction between particles is realised only by photons (by electromagnetic radiation). In this case $m_x = 0$ and then $m_y = m_f$, the coupling constant $\bar{\alpha} \rightarrow \infty$.
- An interaction is realised only via messenger particles. In this case $m_f = 0$ and then $m_y = m_x$, the coupling constant $\bar{\alpha} = 0$.

- Both, particles and photons are involved in an interaction (between particles). The special case is for $m_x = m_f$. Mass is therefore $m_y = 2m_x$ and the coupling constant is $\bar{\alpha} = 1$.

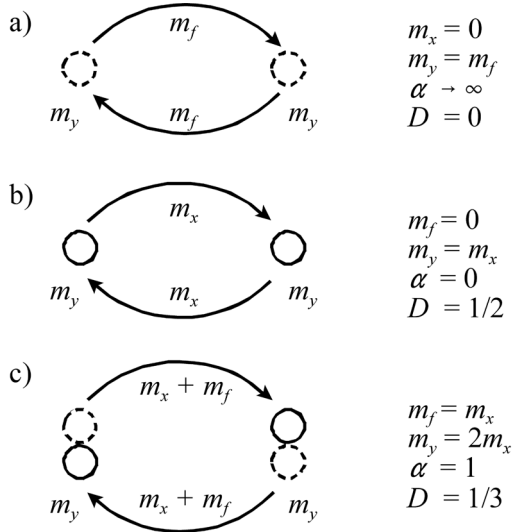


Figure 9 Coupling constant and fractal dimension for a) electromagnetic, b) particle, c) both electromagnetic and particle interaction

Generally speaking, dominant photon interaction is for $m_x > m_f$ and dominant particle interaction is for $m_x < m_f$.

Interactions between quarks. Let us begin with the basic equation of replaceable mechanism between neutron and proton ($n = p + \bar{\nu}_e + e^-$). Let's assume that there exists a similar mechanism between quarks down and up ($d = u + \bar{\nu}_e + e^-$).

It is clear (from Figure 10) that an inverse coupling constant increases with the mass of interacting elements. The following conclusions can thus be formulated:

- Quarks with smaller mass, when $\bar{\alpha}_q < 1$ are more stable.
- The bigger the mass of quarks the more substantial participation of the photons in the interaction (system needs energy) – endothermic reaction.
- Particle exchange (quarks and leptons) dominates for particles with mass smaller than ~ 7.5 MeV (up and down quarks).

Interactions between mesons (pions and kaons). Inverse coupling constants calculated from the hadronic and semileptonic modes of experimental outcomes are presented in Figure 10. It is evident, that the coupling constants of hadronic-mode-interactions are $\alpha > 1$ (predominant photon interactions) and of semileptonic-modes are $\alpha < 1$ (predominant particle interactions).

The logarithmic dependencies of inverse coupling constants fractal dimensions and mass of mesons on the total mass of reacting quarks (and leptons) are shown in Figure 10.

By contrast, for the third case (upper decreasing dependency) is the inverse coupling constant $\bar{\alpha} \approx 0.1 - 10$. These values are typical for strong interactions. The range of such interactions decreases with the total mass of interacting particles.

Interactions between baryons. The experimental and theoretical values of masses were computed for current quarks and their antiparticles. The logarithmic dependencies of the inverse coupling constants, fractal dimensions and mass of baryons on the total mass of reacting quarks, together with dependencies of quarks and mesons are shown in Figure 10.

It is clear from *Figure 10* that the dependency of the inverse coupling constant of baryons on the total mass of participating particles decline similar to the mesons. Its values are circa an order of magnitude higher. The bigger is the mass of baryons, the smaller is the inverse coupling constant. The values of the constant smaller than one are characteristic for charm baryons. The interaction is therefore mainly mediated by particles.

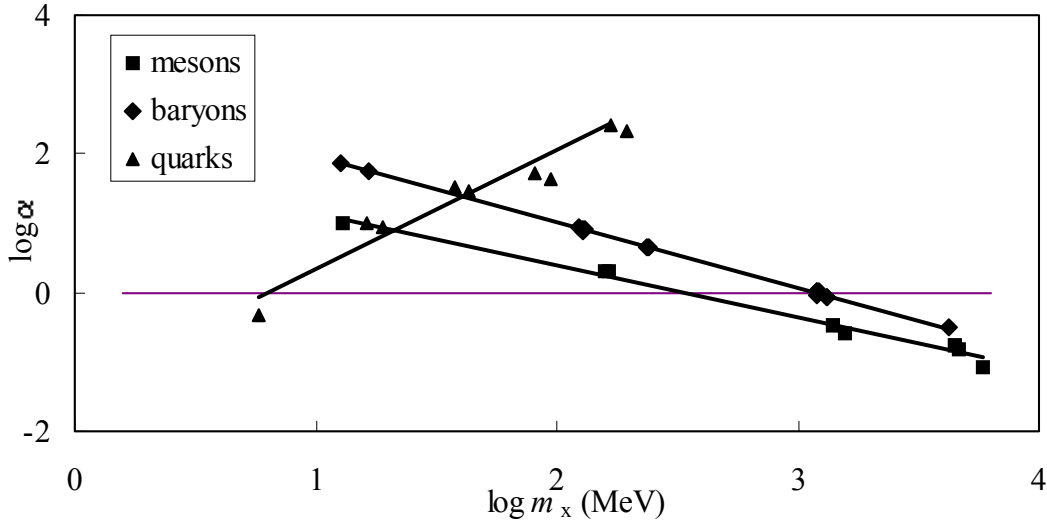


Figure 10 Dependencies of coupling constants of quarks (\blacktriangle), mesons (\blacksquare) and baryons (\blacklozenge) on the current mass of interacted quarks

6. TERMAL FIELD

Heat transfer can be carried out via three basic ways: heat conduction, heat convection and heat radiation. The first and the second eventuality take place in the matter substance, whereas the third one plays a role in vacuum. Generally (in the fractal matter substance) can be the heat transfer mediated by all of the styles together.

The Fourier's laws usually describe *the heat conduction* in solids; their stationary forms can be written with the help of equations [22]

$$q_0(r) = \text{div } \mathbf{q} = \text{div}(-\lambda \text{grad } T) = -\lambda \Delta T, \quad (6.1)$$

where $q_0(r)$ is the specific yield of the heat source (in $\text{J} \cdot \text{m}^{-3} \cdot \text{s}^{-1}$), $\mathbf{q}(r)$ is the density of heat flow rate (in $\text{J} \cdot \text{m}^{-2} \cdot \text{s}^{-1}$), $T(r)$ is the temperature (in K) and λ is the constant thermal conductivity (in $\text{J} \cdot \text{K}^{-1} \cdot \text{m}^{-1} \cdot \text{s}^{-1}$) and

$$\lambda = c_p \rho a = C_p a, \quad (6.2)$$

where c_p is the specific heat capacity after constant pressure (in $\text{J} \cdot \text{K}^{-1} \cdot \text{kg}^{-1}$), C_p is the density of heat capacity (in $\text{J} \cdot \text{K}^{-1} \cdot \text{m}^{-3}$), ρ is the mass density (in $\text{kg} \cdot \text{m}^{-3}$) and a is the coefficient of thermal diffusivity of the body (in $\text{m}^2 \cdot \text{s}^{-1}$).

The **heat convection** in fluids (liquids and gases) can be described analogically. It arises from different temperatures of molecules in liquids (e.g. during heating). The motion of the molecules (diffusion) can be described using Fick's laws [23]

$$q_m(r) = \text{div } \mathbf{q}_m = \text{div}(-D \text{grad } \rho) = -D \Delta \rho, \quad (6.3)$$

where $q_m(r)$ is the specific yield of the heat source (in $\text{kg} \cdot \text{m}^{-3} \cdot \text{s}^{-1}$), $\mathbf{q}_m(r)$ is the density of mass flow rate (in $\text{kg} \cdot \text{m}^{-2} \cdot \text{s}^{-1}$), $\rho(r)$ is the mass density (in $\text{kg} \cdot \text{m}^{-3}$) and D is the diffusion coefficient (in $\text{m}^2 \cdot \text{s}^{-1}$), which is formally equivalent to the coefficient of thermal diffusivity a (6.2).

The **heat radiation** in vacuum can be described in the same manner using the Kirchhoff radiation law [24]. It reads

$$q_e(r) = \text{div } \mathbf{H}_e = \text{div}(-a \text{grad } w) = -a \Delta w, \quad (6.4)$$

where $q_e(r)$ is the specific power density of the heat source (in $\text{J} \cdot \text{m}^{-3} \cdot \text{s}^{-1}$), $\mathbf{H}_e(r)$ is the radiant excitance (in $\text{J} \cdot \text{m}^{-2} \cdot \text{s}^{-1}$), $w(r)$ is the radiant energy density (in $\text{J} \cdot \text{m}^{-3}$) and a is the coefficient of thermal diffusivity in the vacuum (in $\text{m}^2 \cdot \text{s}^{-1}$).

A uniform mathematical system describing the heat transfer independently on the properties of the matter (solid-state, liquid, gas and vacuum) can be formulated. Fractal dimension and fractal measure will be the only parameters distinguishing the differences. Let's choose the density of heat capacity C_p as a basic quantity. From the Stefan-Boltzmann radiation law

$$H_e = \sigma T^4, \quad \sigma = \frac{\pi^2 k^4}{60c^2 \hbar^3} = 5.67051 \cdot 10^{-8} \text{ J} \cdot \text{s}^{-1} \cdot \text{m}^{-2} \cdot \text{K}^{-4}, \quad (6.5)$$

where $k = 1.380658 \cdot 10^{-23} \text{ J} \cdot \text{K}^{-1}$ is Boltzmann constant, $\hbar = 1.05457266 \cdot 10^{-34} \text{ J} \cdot \text{s}$ is the modified Planck's constant and $c = 2.99792458 \cdot 10^8 \text{ m} \cdot \text{s}^{-1}$ is the speed of light in vacuum, it was found that the change of the heat capacity C_p (in $\text{J} \cdot \text{K}^{-1} \cdot \text{m}^{-3}$) depending on temperature in fractal environment can be described as

$$C_p = c_p \rho = \frac{\lambda}{a} = -\frac{k^2}{\hbar c} \Delta T. \quad (6.6)$$

If the heat density is defined as [5] $w = C_p T = c_p \rho T = \lambda T/a$ and using the Eq. (6.6), one obtain (provided that $\lambda/a = \text{const.}$)

$$q_e(r) = C_p \frac{\lambda \hbar c}{k^2} = -a \Delta w, \quad (6.7)$$

which is Eq. (6.4) describing the properties of the heat radiation.

The substitution in this Eq. (6.7) for $aw = \lambda T$ (provided that $\lambda/a = \text{const.}$) one derives

$$q_0(r) = C_p \frac{\lambda \hbar c}{k^2} = -\lambda \Delta T \quad (6.8)$$

which is *Eq. (6.1)* describing the properties of the heat conduction.

The substitution in *Eq. (6.7)* for $aw = c_p \rho T$ (provided that $c_p T = \text{const.}$, i.e. the system is in the heat equilibrium) we derive

$$q_m(r) = C_p \frac{\lambda \hbar c}{k^2} = -c_p T \Delta \rho \quad (6.9)$$

which is *Eq. (6.3)* describing the properties of the heat convection (apart from the constant).

The analysis above shows that *Eq. (6.6)* allows to unified the description of the heat transfer properties assuming that structures transferring the heat are of a fractal nature [4], [5]. In papers [4], [5] the density of fractal physical quantity $C(r)$ in E -dimensional Euclidean space E_n ($E = n$) (the density of heat capacity in $\text{J.K}^{-1} \cdot \text{m}^{-E}$) was defined as

$$C_p(r) = k K r^{D-E}, \quad (6.10)$$

where $n(r)$ is the coverage of space – concentration and distribution of particles, $k = 1.380658 \cdot 10^{-23} \text{ J.K}^{-1}$ is the quantum of heat capacity (Boltzmann constant), r is the radius of elementary quantity, K the fractal measure (in m^{-D}) and D is the fractal dimension. It is apparent already from this equation that in equally filled space ($D = E$) the heat density is constant, while for the point source of the heat ($D = 0, E = 3$) the heat density decreases with the distance from the source with third power.

For radial temperature field we can the dependence of temperature on radius using by (10) write

$$T_r = -\frac{\hbar c}{k} \cdot \frac{K r^{D-E+2}}{D(D-E+2)}, \quad (6.11)$$

From this equation it is obvious that in the space with constant density of the heat capacity $C(r)$ (i.e. for $D = E$) the temperature increases with second power. In the case of point-like source of the heat radiation (i.e. for $D = E$) the temperature decreases with the distance by $1/r$. Assuming that there is linear source of heat (hot wire, $D = E - 2, E = 3$), the temperature is constant over the whole space.

From the density of the heat capacity *Eq. (6.10)* and from the temperature *Eq. (6.11)* the density of energy (in J.m^{-E})

$$w(r) = C(r)T_r(r) = n(r)kT_r(r) = -\hbar c \frac{K^2 r^{2(D-E+1)}}{D(D-E+2)} \quad (6.12)$$

respectively

$$w(T_r) = K \cdot \left[\frac{D(E-D-2)}{K\hbar c} \right]^{\frac{E-D}{E-D-2}} \cdot (kT_r)^{\frac{2(E-D-1)}{E-D-2}} = KkT_r \left[\frac{kT_r D(E-D-2)}{K\hbar c} \right]^{\frac{E-D}{E-D-2}} \quad (6.13)$$

can be determine.

The radiation of a point source of heat (black body) ($D = 0$, $E = 3$) is usually described using the well-known Stefan-Boltzmann's law

$$w \approx \frac{k^4 D^3}{K^2 \hbar^3 c^3} T_r^4 = \frac{\pi^2}{60} \frac{k^4}{\hbar^3 c^3} T_r^4 = \frac{\sigma}{c} T_r^4, \quad (6.14)$$

where $K^2/D^3 = 60/\pi^2$, $\sigma = (\pi^2 k^4)/(60c^2 \hbar^3)$, see Eq. (6.5).

On the other hand, the homogeneously spread matter (e.g. ideal gas) ($D = 3$, $E = 3$) is described as

$$w \approx KkT_r. \quad (6.15)$$

This is essentially the energy of the gas unitary volume (ideal gas pressure).

Let's first consider the properties of heat transfer in the three-dimensional space ($E = 3$) just for the fractal dimensions $D \in \langle 0,1 \rangle$ of the heat source. In this case, the heat density (Eq. (6.13)) can be written using generalised Planck radiation law

$$w(T_r) = \frac{K(K\hbar c)}{D(1-D)} \cdot \left(\frac{kT_r D(1-D)}{K\hbar c} \right)^{\frac{2(2-D)}{1-D}} = KkT_r \left[\frac{kT_r D(1-D)}{K\hbar c} \right]^{\frac{3-D}{1-D}}, \quad (6.16)$$

The power of the temperature T_r can gain values at interval $\langle 4, \infty \rangle$.

The *Figure 11* shows the dependency of the energy density on fractal dimension for a specific number of oscillators ($K \approx 2.2 \times 10^6 \text{ m}^{-3}$). The parameter of the dependences is temperature. Its values were chosen to allow comparison with experimentally gained values for the Sun. According to [6] it can be assumed that the interaction (radiation) at lower energy densities is mediated by fotons ($D \rightarrow 0$), while at higher energy densities is mediated by particles ($D \rightarrow 1$). The temperature of the maximum of these dependences can be written

$$T_m = \frac{K\hbar c}{kD_m(1-D_m)} \cdot \exp \left[-\frac{(3-D_m)(1-2D_m)}{2D_m} \right], \quad (6.17)$$

where D_m is the fractal dimension of the maximum position. Using Eq. (6.16) it is also possible to obtain the dependency of maximal energy density w_m (of the temperature) on the fractal dimension value

$$w_m = \frac{K(K\hbar c)}{D_m(1-D_m)} \cdot \exp \left[-\frac{(3-D_m)(2-D_m)(1-2D_m)}{D_m(1-D_m)} \right]. \quad (6.18)$$

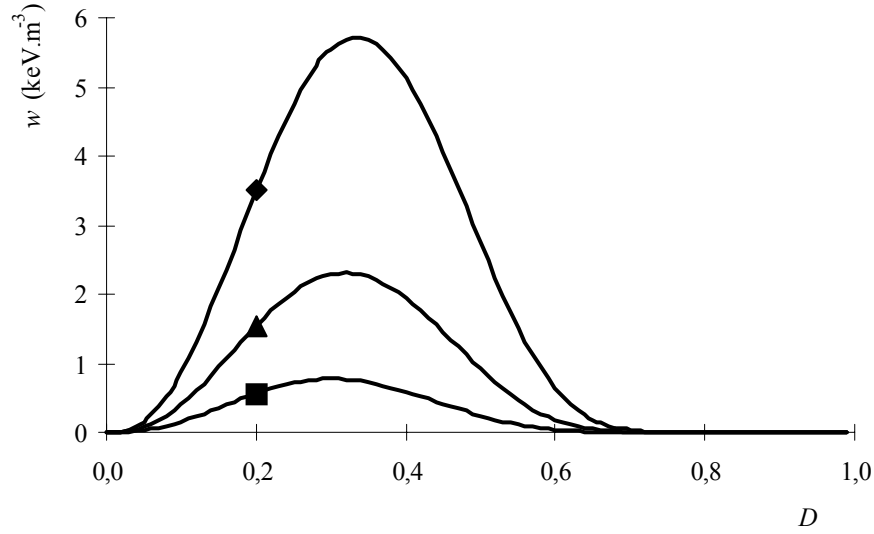


Figure 11 The dependency of the energy density of heat oscillators on their fractal dimension plotted for three different temperatures (■ $T = 4000$ K, ▲ $T = 5000$ K, ◆ $T = 6000$ K) and constant number of oscillators ($K = 2.2 \times 10^6 \text{ m}^{-3}$).

The integration of dependencies from Figure 11 (Eq. (6.13)) over the fractal dimension D allows to obtain total (mean) energy density of all oscillators

$$w_s = \int_0^1 w dD = K k T_r \int_0^1 \left[\frac{k T_r D(1-D)}{K \hbar c} \right]^{\frac{3-D}{1-D}} dD \quad (6.19)$$

The computed dependency of resultant energy of heat oscillators on their temperature for specific number of oscillators ($K = 2.2 \times 10^6 \text{ m}^{-3}$) is depicted on Figure 12. Dashed line represents asymptotic dependency computed from

$$w_m = \frac{k^4 D_m^3}{K^2 \hbar^3 c^3} T_m^4 = \frac{\pi^2 k^4}{60 \hbar^3 c^3} T_m^4 \quad (6.20)$$

This dependency represents the Stefan – Boltzmann's radiation law. The Steepness of its logarithmic dependency for $D_m \rightarrow 0$ can be determine from Eq. (6.18) and Eq. (6.18) as

$$\frac{d \ln(w_m)}{d(\ln T_m)} \approx \frac{6 - D_m}{3/2 - D_m} \approx 4 \quad (6.21)$$

Analysing relations (6.18) and (6.18) one can learn that for temperature $T_m \rightarrow 0$ the fractal dimension is also $D_m \rightarrow 0$. The objects therefore behave as an ideal mass point and the interaction is mediated only by the electromagnetic interaction (photons) ($\bar{\alpha}_w \rightarrow \infty$) [6]. The energy density will also come close to zero ($w_m \rightarrow 0$).

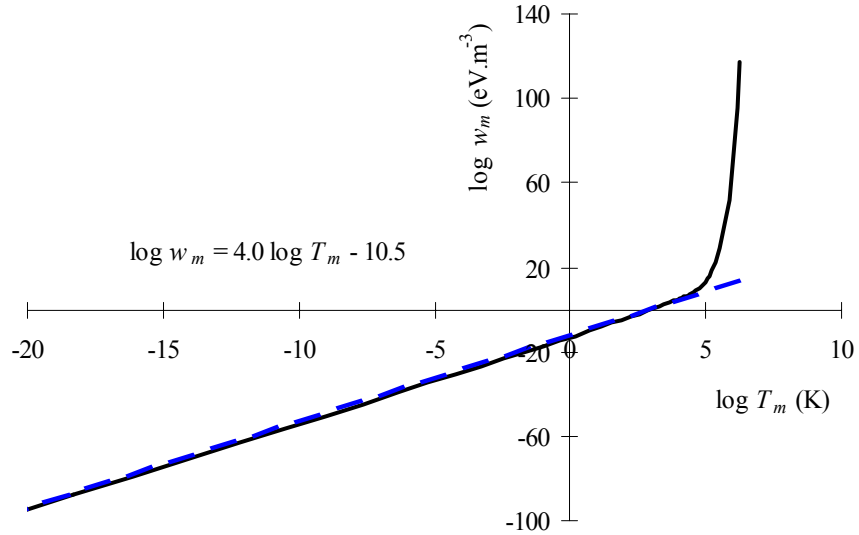


Figure 12 The dependency of energy density of heat oscillators on their temperature computed for constant number of oscillators ($K = 2.2 \times 10^6 \text{ m}^{-3}$). The dashed line represents the asymptotic value of $w_m \approx \sigma T^4$ (6.20)

A mass begins to gain volume as the temperature rises and the fractal dimension of the structure increase. The mass density will be spread out in accordance with the Planck's radiation law. The wavelength and the fractal dimension are connected by the following equation:

$$\bar{\alpha}_w = \frac{\lambda}{\lambda_0} = \frac{1-D}{D}, \quad (6.22)$$

where $\bar{\alpha}_w = \bar{\alpha} + 1$ is the inverse coupling constant of the mass energy ($\bar{\alpha}$ is the inverse coupling constant of energy [6]), λ_0 is the wavelength for fractal dimension $D = 1/2$. For this wavelength is the $w \approx T^6$. In this case according to [6] is the interaction mediated equally both by the photons and also by the particles (objects with fractal dimension $D = 1/2$ respectively). The most populated are particles having the fractal dimension D_m (see Figure 12).

On the other hand, when $T_m \rightarrow \infty$ the fractal dimension is $D_m \rightarrow 1$ (from the left side) and the inverse coupling constant of mass energy is $\bar{\alpha}_w \rightarrow 0$. Interaction with other objects is mediated only by particles (according to [6]). The mass density gets closer to the limit point at the infinity ($w_m \rightarrow \infty$).

Using Eq. (6.18) and (6.22) we can formulate the Wien's displacement law

$$\lambda_m T_m = \frac{K \lambda_0 \hbar c}{k D_m^2} \cdot \exp \left[- \frac{(3 - D_m)(1 - 2D_m)}{2D_m} \right], \quad (6.23)$$

i.e. dependency of the maximal wavelength of the Planck's radiation law (6.16) on the temperature. Considering Figure 12 and Eq. (6.23) it become obvious that for $D_m \approx 0.31854$, which is the fractal dimension when $K\hbar c/kT \approx K\lambda_0 \approx 1$, is the value of $\lambda_m T_m = \hbar c(1 - D_m)/kD_m \approx 4.89877 \times 10^{-3} \text{ m}$.

Analysing the dependencies expressing the Planck's radiation law, similar results are obtained

$$w_\nu = \frac{dw_s}{d\nu} = \frac{\lambda^2}{c} \frac{dw_s}{d\lambda} = \frac{2\pi h \nu^3}{c^3 [\exp(h\nu/kT) - 1]} = \frac{2\pi h}{\lambda^3 [\exp(hc/\lambda kT) - 1]}, \quad (6.24)$$

where $\nu = c/\lambda$ is the frequency of the electromagnetic wave. Considering $dw_\nu/d\nu = d^2 w_s/d\nu^2 = 0$ one can derive relation between the maximal wavelength of the function $\lambda_m = c/\nu_m$ and temperature T_m (so-called Wien's displacement law). The value $\lambda_{\nu m} T_m \approx 5.0941 \times 10^{-3} \text{ m}$ is very close to the value computed by our mathematical apparatus for $K\hbar c = kT_m$.

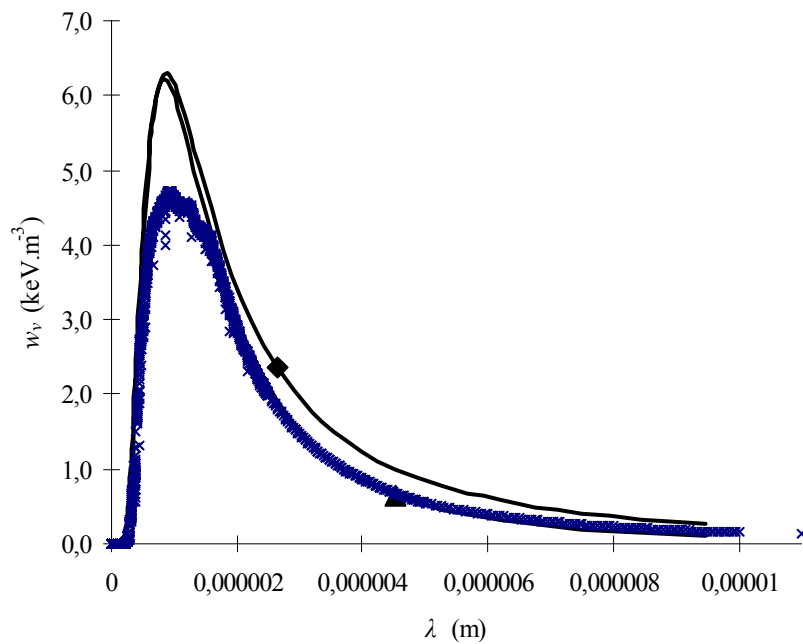


Figure 13 The spectral energy density of heat oscillators computed for temperature $T = 5800 \text{ K}$ and $K = 2.53 \times 10^6 \text{ m}^{-3}$ using the Planck's radiation law (\blacklozenge) and dependency defining the energy density of fractal structure (\blacktriangle). The results are compared with measured values of the Sun. See text for further discussion.

For fractal dimensions within the interval $D \in (1, 3)$ the $D(1 - D)$ term in Eq. (6.16) is minus and relation for energy density, which in this case represents the gas pressure (i.e. $w(T_r) = p(T_r)$), has to be rewritten into

$$p(T_r) = KkT_r \left(-1\right)^{\frac{3-D}{1-D}} \left[\frac{kT_r D(D-1)}{K\hbar c} \right]^{\frac{3-D}{1-D}}, \quad (6.25)$$

where using the Moivre's theorem

$$\left(-1\right)^{\frac{D-3}{D-1}} = \exp\left(j\delta \frac{D-3}{D-1}\right) = \cos\left(\frac{D-3}{D-1}\delta\right) + j \cdot \sin\left(\frac{D-3}{D-1}\delta\right). \quad (6.26)$$

We can see, that from these relations, the energy density can generally gains complex values. The real values can the energy density gains for discrete values of fractal energy $D = (n+2)/n$, where $n=1,2,3,\dots$ (normal gas component). The imaginary values when fractal dimension gains $D = (2n+5)/(2n+1)$ (tangential component of gas pressure; connected with tangential tension between molecules, so-called cohes pressure).

According to (6.12) and using Eq. (6.25) it is also possible to express the concentration of molecules of the gas [23]

$$n(T_r) = K \left(-1\right)^{\frac{3-D}{1-D}} \left[\frac{kT_r D(D-1)}{K\hbar c} \right]^{\frac{3-D}{1-D}}, \quad (6.27)$$

By fusion of Eq. (6.25) and (6.26) we derive

$$p = nkT_r, \quad (6.28)$$

which is a relation defining the gas pressure [23] (the ideal gas equation of unit volume of the gas respectively). When the fractal dimension is $D=3$ it can be expressed as

$$p_{id} = \frac{RT_r}{V_M} = KkT_r, \quad (6.29)$$

where $V_m = N_A/K$ is the molar gas volume, $R = k N_A$ is the molar gas constant, N_A is the Avogadro constant, which represents the ideal gas equation.

To describe the behaviour of real gases it is more practical to use the so-called compressibility factor. With the help of Eq. (6.27) and (6.29), it can be defined by the equation

$$Z = \frac{p}{p_{id}} = \frac{pV_M}{RT_r} = \left(-1\right)^{\frac{D}{1-D}} \left[\frac{kT_r D(D-1)}{K\hbar c} \right]^{\frac{3-D}{1-D}}. \quad (6.30)$$

It is apparent, that some specific fractal dimensions leads to the real solution (there are no cohesion forces between molecules). Positive values are equal to the pressure, which leads to the expansion of the gas ($D=3/1, 5/3, 7/5, \dots$). Negative values,

however, imply gas compression ($D = 2/1, 3/2, 4/3, \dots$). These levels are moving towards – assuming continuous character – for fractal dimensions $D \rightarrow 1$ (from the right-hand side). At the same time, the size of the compressibility factor mounts up.

The size of the compressibility factor can be determine using (6.30), ((6.25) respectively) with the help of following equations

$$Z = \left[\frac{kT_r D(D-1)}{K\hbar c} \right]^{\frac{3-D}{1-D}} = \left[\frac{p \cdot D(D-1)}{K(K\hbar c)} \right]^{\frac{3-D}{2(2-D)}} = \left[V^* \right]^{\frac{D-3}{3}}, \quad (6.31)$$

The dependency of the compressibility factor size on the fractal dimension at three different temperatures is plotted in *Figure 14*. Assuming that the temperature is low the compressibility factor has a growing tendency straight away from the beginning (when the fractal dimension decreases). In the other cases the compressibility factor begins to grow only after previous decreasing period. At critical temperature the system ($K\hbar c = kT_r$) gains $Z = 1$ (except for the case of the ideal gas $D = 3$) also for the fractal dimension $D = \phi = 1.618033989$, where ϕ is the golden mean value of El Nashie's golden mean field theory. The minimum of function (6.31) determines so-called critical temperature T_m (similarly to (6.17))

$$T_m = \frac{K\hbar c}{kD_m(D_m-1)} \cdot \exp \left[-\frac{(3-D_m)(1-2D_m)}{2D_m} \right], \quad (6.32)$$

and its corresponding compressibility factor (6.31)

$$Z_m = \exp \left[-\frac{(3-D_m)^2(1-2D_m)}{2D_m(1-D_m)} \right], \quad (6.33)$$

and critical pressure (similarly to Eq. (6.18))

$$p_m = \frac{K(K\hbar c)}{D_m(D_m-1)} \cdot \exp \left[-\frac{(3-D_m)(2-D_m)(1-2D_m)}{D_m(1-D_m)} \right] \quad (6.34)$$

The value of the compressibility factor is equal to one for fractal dimension $D = 3$.

It is possible to establish from the dependency shown in *Figure 14a* and the condition

$$\left(\frac{dZ}{dp} \right)_{T_B} = \left(\frac{dZ}{dD} \right)_{T_B} \left(\frac{dD}{dp} \right)_{T_B} = 0 \quad (6.35)$$

the so-called Boyle temperature (temperature at which real gasses behave as the ideal one - when the pressure is low or the volume is small). The minimum of (6.31) function arise when the fractal dimension $D = 3$. According to Eq. (6.32) we can thus write: $Z_B = 1$, $T_B = K\hbar c/6k$, $p_B = K(K\hbar c)/6$. Typical values are listed for

several gasses in *Table III* [23]. The last row contains the limit temperature $K_B \hbar c / k$, which represents the point when real gasses behave almost as the ideal ones.

The function (6.31) has a minimum at smaller fractal dimension than is the topological dimension ($D < 3$) when the temperature is lower than the critical Boyle temperature. This minimum corresponds to the critical parameters of a real gas; see *Table IV*.

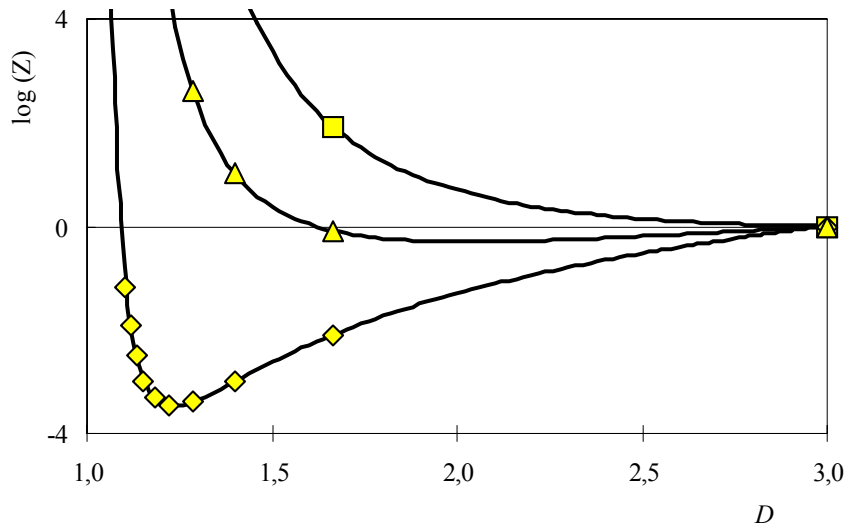


Figure 14 The dependency of compressibility factor size on fractal dimension plotted for three different temperatures ■ $T = 50000$ K, ▲ $T = 5000$ K (i.e. for $K \hbar c \approx kT_r$), ◆ $T = 500$ K

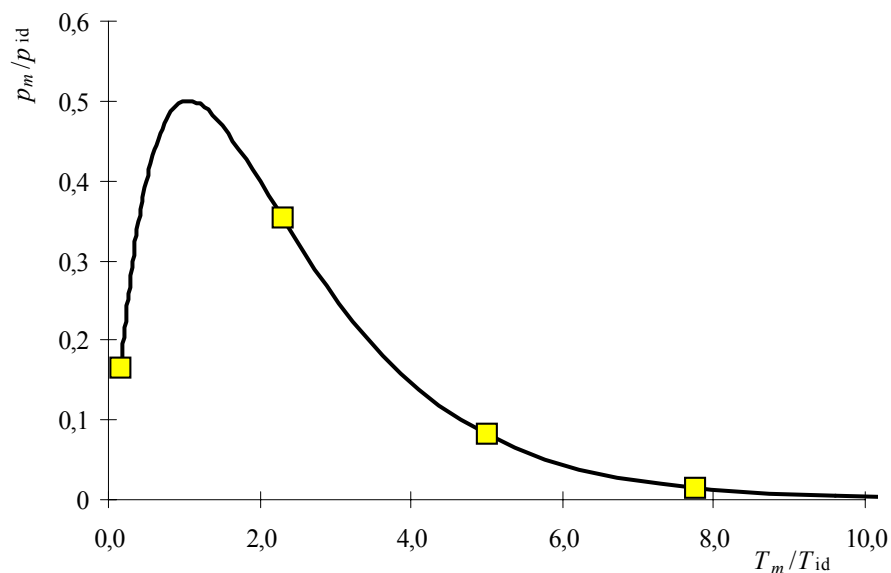


Figure 15 The dependency of the compressibility factor (6.30) on relative temperature computed for given number of molecules – oscillators ($K = 2.2 \times 10^8 \text{ m}^{-3}$).

Table III. The Boyle's constants of some representative gasses [23] and their corresponding fractal parameters

	M_r	p_B (Pa)	T_B (K)	V_B (m ³ .mol ⁻¹)	Z_B	D_B (-)	K_B (m ⁻³)	$K_B\hbar c/k$ (K)
Ar	39.95	$3.689 \cdot 10^9$	411.5	$9.274 \cdot 10^{-7}$	1.000	3.000	$1.08 \cdot 10^6$	2469.0
CO ₂	44.01	$1.113 \cdot 10^{10}$	714.8	$5.339 \cdot 10^{-7}$	1.000	3.000	$1.87 \cdot 10^6$	4288.8
He	4.003	$1.117 \cdot 10^7$	22.64	$1.686 \cdot 10^{-5}$	1.000	3.000	$5.93 \cdot 10^4$	135.8
O ₂	31.999	$3.589 \cdot 10^9$	405.9	$9.402 \cdot 10^{-7}$	1.000	3.000	$1.06 \cdot 10^6$	2435.4

Table IV. The critical constants of some representative gasses [23] and their corresponding fractal parameters

	M_r	p_c (Pa)	T_c (K)	V_c (m ³ .mol ⁻¹)	Z_c	D_c (-)	K_{cZ} (m ⁻³)	$K_{cZ}\hbar c/k$ (K)
Ar	39.95	$4.800 \cdot 10^6$	150.7	$7.53 \cdot 10^{-5}$	0.292	1.820	$2.34 \cdot 10^4$	53.6
CO ₂	44.01	$7.290 \cdot 10^6$	304.2	$9.40 \cdot 10^{-5}$	0.274	1.802	$2.91 \cdot 10^4$	66.7
He	4.003	$2.260 \cdot 10^5$	5.21	$5.78 \cdot 10^{-5}$	0.305	1.833	$5.05 \cdot 10^3$	11.6
O ₂	31.999	$5.014 \cdot 10^6$	154.8	$7.80 \cdot 10^{-5}$	0.308	1.837	$2.37 \cdot 10^4$	54.3

From the temperature dependency on the fractal dimension it is apparent that the temperature increases with decreasing fractal dimension. At $D_m \rightarrow 1$ (from the right side) the temperature increases over all limits ($T_m \rightarrow \infty$). When $D_m = 3$, it is equal to the Boyle temperature $T_B = K\hbar c/6k$. The dependency of pressure on the fractal dimension (6.34) has a maximum at $D_m = 2$. The position of compressibility factor maximum can be also derived in the same manner $D_m \approx 2.0269$ (6.33).

7. STEADY STATE ELECTRIC CURRENT

Dependencies (3.14) – (3.17) were found in the study of electrical properties of semiconductors [18], [19] and [20]. First of them is dependence of field intensity on voltage for plane-parallel current flow geometry

$$E_L = (2 - \gamma)U_L/L, \quad (7.1)$$

where γ is a coefficient related to the steepness of the volt-ampere characteristic $\gamma = d \ln U_L / d \ln j$ and L is distance between contacts. The equation has to be modified for any other geometry than Euclidian space

$$E_L = (2 - E\gamma)U_L/L. \quad (7.2)$$

Using equations (3.14) and (7.2) it becomes possible to define coefficient γ as $\gamma = (E - D)/E$. The space charge in the semiconductor arises when fractal dimension $D \in \langle 0, E \rangle$, coefficient γ then changes in interval $\gamma \in \langle 0, 1 \rangle$. In this case the current density j_{fL} will be proportional to flow of energy w_{fL} in transport (conduction or valence) band of semiconductor

$$j = \mu i_{fL} = \mu \rho_{fL} E_L = e \mu n_{fL} E_L = e \mu n_{fL} (2 - E\gamma)U_L/L, \quad (7.3)$$

where μ is mobility and n_{jL} is concentration of free carriers.

For $D = E - 1$ there will be homogenous field in the matter (see *Table I*) and the contact will be ohmic ($\gamma = 1/E$). For $D = E - 2$ the field in the matter will be zero and the contact will be blocking ($\gamma = 2/E$) and for $D = E$ the contact will be ideally injecting ($\gamma = 0$).

Other electrical properties of the materials can be described using coefficient γ as well. For example:

- the charge density and the total charge in space

$$\rho_L = \frac{eK}{L^{E\gamma}}, \quad Q_L = \frac{eK}{1-\gamma} \cdot \frac{1}{L^{E(1-\gamma)}}, \quad (7.4)$$

- the intensity and the potential of electric field

$$E_L = \frac{eK}{\epsilon_0\epsilon_r} \cdot \frac{L^{1-E\gamma}}{E(1-\gamma)}, \quad U_L = -\frac{eK}{\epsilon_0\epsilon_r} \cdot \frac{L^{2-E\gamma}}{E(1-\gamma)(2-E\gamma)}. \quad (7.5)$$

- the differential specific capacity of electric field

$$c = \frac{\rho}{U_L} = -\epsilon_0\epsilon_r \frac{E(1-\gamma)(2-E\gamma)}{L^2}. \quad (7.6)$$

- the dependency of concentration of trapped carriers on voltage (on field intensity)

$$n_{sL} = \frac{w}{eU_L} = E(1-\gamma)(2-E\gamma)\epsilon_0\epsilon_r U_L / eL^2, \quad (7.7)$$

or using (7.6)

$$n_{sL} = E(1-\gamma)\epsilon_0\epsilon_r E_L / eL. \quad (7.8)$$

The equation (7.3) combined with (7.7) gives then

$$j = E(1-\gamma)(2-E\gamma)^2 \mu\epsilon_0\epsilon_r \theta U_L^2 / L^3, \quad (7.9)$$

or using (7.6)

$$j = E(1-\gamma)\mu\epsilon_0\epsilon_r \theta E_L^2 / L, \quad (7.10)$$

where $\theta = n_{jL} / n_{sL}$ is coefficient defined as ratio of concentration of the free charge to concentration of the trapped charge.

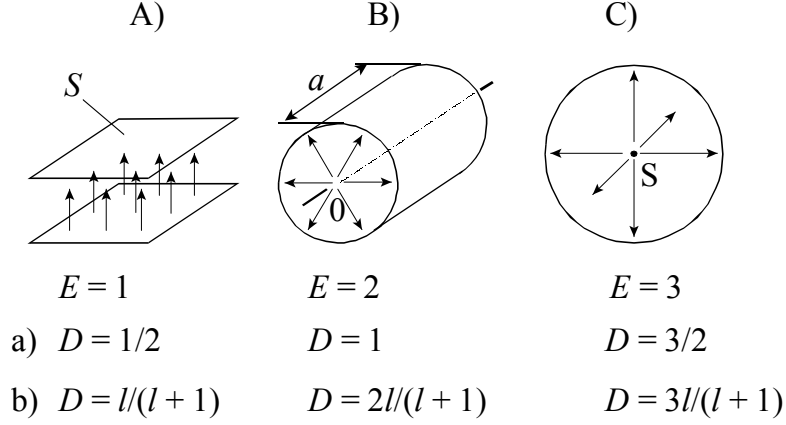


Figure 16 Current flow geometry: A) plane-parallel, B) cylindrical, C) spherical and their fractal dimensions for space charge regime: a) shallow traps and b) exponential distributions of traps

Equation (7.7) and (7.8) describes the transport of the charge in E-dimensional space. Special cases are for (see Figure 16)

- plane-parallel current flow geometry (for $E = 1$), $I = Sj$, S is an area of planes,
- cylindrical current flow geometry (for $E = 2$), $I = 2\pi Laj$, a is a length of cylinder,
- spherical current flow geometry (for $E = 3$), $I = 4\pi L^2j$.

Figure 16 is formally similar to the Figure 8. The difference between them is in description of movement of the electric charge in one, two or three-dimensional space in Figure 16 and of relative geometry of the electrode in 3-dimensional space in Figure 8.

Ohmic contact regime occurs when there is homogenous electric field present in the whole volume of examined matter ($D = E - 1$). It can be derived using equation (7.2) that such situation occurs for $\gamma = 1/E$, when intensity of the electric field

$$E_L = U_L/L \quad (7.11)$$

is independent to the dimension of the fractal structure (the distance between contacts of electrodes L). The equation for ohmic current (7.3) can be then written as

$$j_\Omega = e\mu n_{fL0} E_L = e\mu n_{fL0} U_L/L \quad (7.12)$$

According to the commonly accepted band model, the concentration of thermally generated electrons may be described within the Boltzmann statistics

$$n_{fL0} = N_b \exp\left(\frac{E_{c0} - E_{F0}}{kT}\right) \quad (7.13)$$

Here, N_b is the effective density of states in the band (density of extended states), E_{c0} is the energy of the band edge in an isolated sample, and E_{F0} is the energy of the “thermodynamic” Fermi level; both energies are measured with respect to an external reference level (vacuum level, in this case). Note that at equilibrium n_{fL0} ,

E_{c0} and E_{F0} are all constant within the sample. For current, one can write the equation

$$I_{\Omega} = e\mu n_{fL0} E_L S \quad (7.14)$$

where S is the sample area. For a planar sample, i.e. the homogeneous field, $F_L = U_L/L$, where U_L is the applied voltage and L is the sample thickness. However, generally the electric field strength strongly depends on electrode configurations and shapes.

Space charge regime occurs when homogenous density of charge occurs in the whole volume of the examined sample ($D = E$). This situation occurs for $\gamma = 0$, as shown in (7.2), when density becomes independent to the dimension of the fractal structure (distance between contacts of the electrodes L). The defining voltage or field intensity is then obtained by combination of the equations (7.8) and (7.9), or (7.10) when allowed states in the semiconductor are fully filled (TFL - trap field limit regime)

$$E_{TFL} = \frac{en_{fL0}L}{\epsilon_0\epsilon_r\theta} \cdot \frac{1}{E(1-\gamma)} = \frac{en_{fL0}L}{E\epsilon_0\epsilon_r\theta} \quad (7.15)$$

$$U_{TFL} = \frac{en_{fL0}L^2}{\epsilon_0\epsilon_r\theta} \cdot \frac{1}{E(1-\gamma)(2-E\gamma)} = \frac{en_{fL0}L^2}{4E\epsilon_0\epsilon_r\theta} \quad (7.16)$$

where $n_{sL} = n_{fL} + N_t$ and $\theta = (n_{sL} - N_t)/n_{sL}$, N_t is concentration of traps.

Concentration of trapped charge n_{sL} depends on concentration of free charge n_{fL} and on a character of states on which the charge is trapped

- for perfect trap free insulator is $n_{fL} = n_{sL}$ and $\theta = 1$,
- for perfect insulator with shallow traps is $n_{fL} = K \cdot n_{sL}$ and $\theta = K = N_c / N_t \cdot \exp[(E_t - E_c) / kT]$, where N_c is effective density of the states in the conduction band, E_c the energy of the bottom edge of the conduction band, N_t is concentration of traps and E_t electron traps level, k Boltzmann's constant and T the temperature in Kelvin,
- for traps distributed in energy (exponential trap distribution) $n_{fL} = N_c (n_{sL} / N_t)^{T_c/T}$ and $\theta = (N_c / N_t^{T_c/T}) n_{sL}^{(T_c/T-1)}$, where $l = m - 1 = (1 - \gamma) / \gamma = T_c/T$

$$j = \mu e N_c [(\epsilon_0\epsilon_r / eN_t) E(1-\gamma)]^{(1-\gamma)/\gamma} (2 - E\gamma)^{1/\gamma} U_L^{1/\gamma} / L^{(2-\gamma)/\gamma}, \quad (7.17)$$

- for vacuum diode

$$j = \epsilon_0\epsilon_r [(2e/m)E(1-\gamma)]^{(1-\gamma)/\gamma} (2 - E\gamma)^{1/\gamma} U_L^{1/\gamma} / L^{(2-\gamma)/\gamma}. \quad (7.18)$$

The following equation is valid for example for vacuum diode in cylindrical settings ($E = 3$, $\gamma = 3/2$, space-charge law, see [21], p. 46)

$$j = \frac{4\sqrt{2}}{9} \epsilon_0\epsilon_r \left(\frac{e}{m}\right)^{1/2} \frac{U_L^{3/2}}{L^2} \quad (7.19)$$

Table V. Current-voltage characteristics for space charge regimes, see [21], p.163

Current flow geometry		Shallow traps: $\theta = N_c / N_t \cdot \exp[(E_t - E_c) / kT]$	Exponential distribution of traps: $N_t(E) = N_0 \cdot \exp[(E - E_c) / kT_c]$, $l = T_c / T > 1$
		$D = E/2$	$D = El/(l + 1)$
		$j = \mu \epsilon_0 \epsilon_r \theta \cdot \frac{E(4-E)^2}{8} \cdot \frac{U_L^2}{L^3}$	$j = \mu e N_c \left[\frac{\epsilon_0 \epsilon_r E l}{e N_t (l+1)} \right]^l \left(2 - \frac{E}{l+1} \right)^{l+1} \frac{U_L^{l+1}}{L^{2l+1}}$
Plane-parallel	$E = 1$	$j = \frac{9}{8} \mu \epsilon_0 \epsilon_r \theta \cdot \frac{U_L^2}{L^3}$	$j = \mu e N_c \left[\frac{\epsilon_0 \epsilon_r l}{e N_t (l+1)} \right]^l \left(\frac{2l+1}{l+1} \right)^{l+1} \frac{U_L^{l+1}}{L^{2l+1}}$
Cylindrical	$E = 2$	$j = \mu \epsilon_0 \epsilon_r \theta \cdot \frac{U_L^2}{L^3}$	$j = \mu e N_c \left[\frac{\epsilon_0 \epsilon_r 2l}{e N_t (l+1)} \right]^l \left(\frac{2l}{l+1} \right)^{l+1} \frac{U_L^{l+1}}{L^{2l+1}}$
Spherical	$E = 3$	$j = \frac{3}{8} \mu \epsilon_0 \epsilon_r \theta \cdot \frac{U_L^2}{L^3}$	$j = \mu e N_c \left[\frac{\epsilon_0 \epsilon_r 3l}{e N_t (l+1)} \right]^l \left(\frac{2l-1}{l+1} \right)^{l+1} \frac{U_L^{l+1}}{L^{2l+1}}$

Typical current-voltage and activation energy-voltage characteristics of polyimide thin film are on the *Figure 17*. The thickness of the measured sample was 500 nm, the the current density j was recalculated for the electrode area of 1.3 mm².

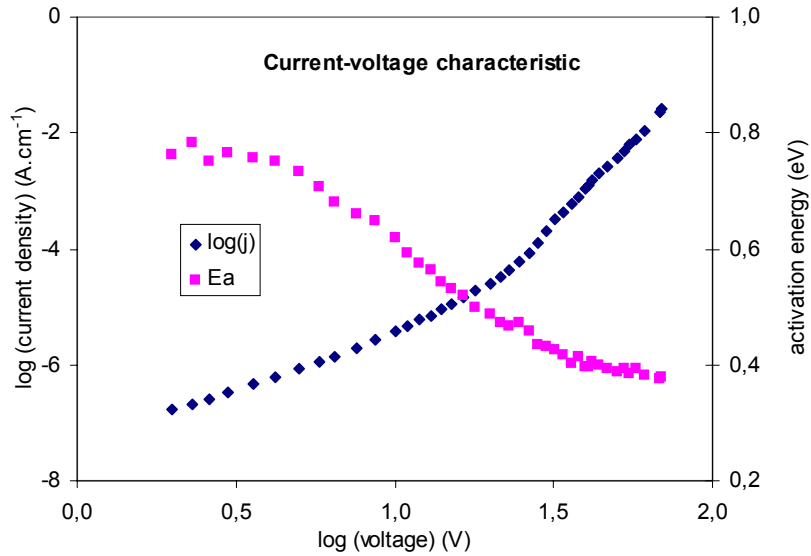


Figure 17 Current-voltage and activation energy - voltage characteristics of polyimide (PI) thin film

From these dependences the slope was determined and with the help of term $\gamma = 1 - D$ the fractal dimension of the charge in one-dimensional space (sandwich sample, $E = 1$) was also obtained, see *Figure 18*. It is evident, that the slope is changing for lower voltages from ohmic mode ($\gamma = 1$) to space charge mode ($\gamma \approx 0.18$). Corresponding fractal dimension is changed opposite, from $D = 0$ (ohmic mode) to $D = 0.82$. Concrete fractal dimension characterize character of distribution charge in the sample. When the fractal dimension is constant, the distribution of charge is not changed.

The density of states in mobility edge (in forbidden gap) of semiconductor can be calculated from the fractal dimension. An exponentially decreasing transport band tail with characteristic temperature $T_c \approx 5000$ K is evident from *Figure 19, Table V*.

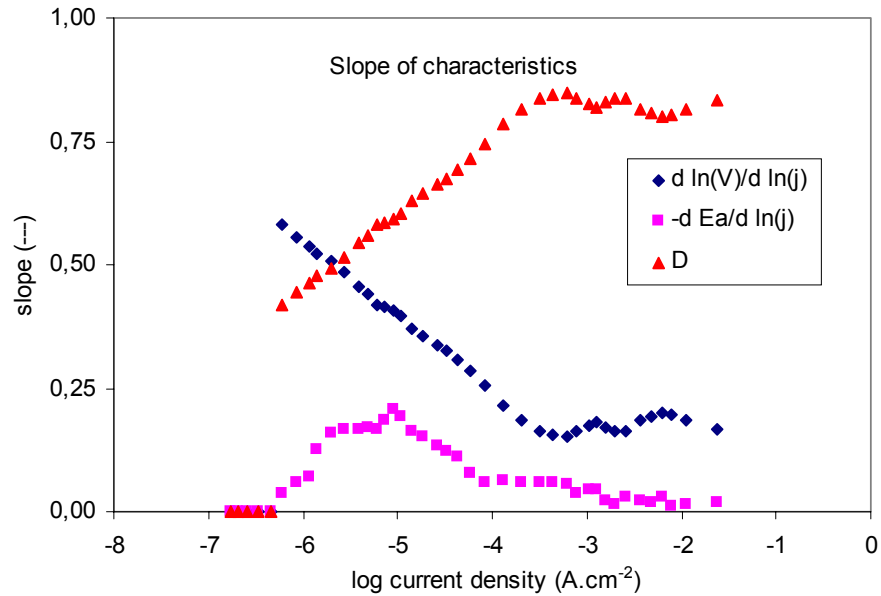


Figure 18 The slope of current-voltage and activation-voltage characteristics and calculated fractal dimension of charge in the sample

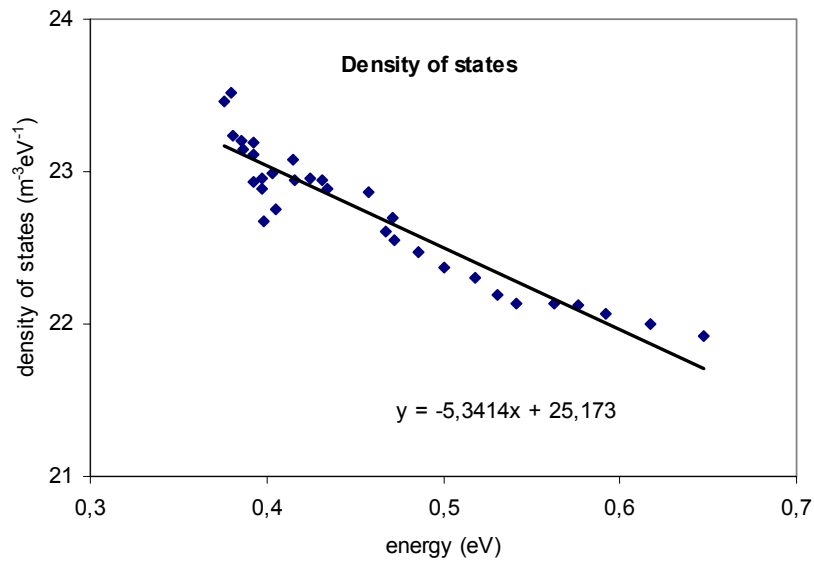


Figure 19 The distribution of density of states in polyimide thin film mobility gap

8. TIME DEPENDENCES OF FRACTAL QUANTITIES

The change of the density of the fractal quantity in time can be in E-dimensional space (for $r = \text{const.}$) defined as

$$\rho_T(t) = \frac{eK}{(c^2t^2 - r^2)^{(E-D)/2}} = \frac{\rho_0}{(t^2/\tau_M^2 - 1)^{(E-D)/2}}, \quad (8.1)$$

where $\rho_0 = eK/(ir)^{E-D}$ is the density of the fractal quantity for time $t = 0$ sec, $i = \sqrt{-1}$ and $\tau_M = r/c$ is the time constant characteristic for the change of the quantity in every point of the space. The simplified equation can be written for times much longer then that of the time constant (i.e for speeds much smaller then that of light c)

$$\rho_T(t) \cong \rho_0 \left(\frac{\tau_M}{t} \right)^{E-D}, \quad (8.2)$$

This equation is often used as approximation of the change of the density (or concentration of the charge) over the time in homogenous electric field ($D = E - 1$). The dependency of the properties above on time change in any point of the space is then obtained in the second case (for $r_T = \text{const.}$)

$$V_r(t) = \frac{V_{r0}}{(t^2/\tau_M^2 - 1)^{(E-D-2)/2}}, \quad E_r(t) = \frac{E_{r0}}{(t^2/\tau_M^2 - 1)^{(E-D-1)/2}}, \quad (8.3)$$

where $\tau_M = r/c$, $V_{r0} = -eK^*/(ir)^{E-D-2}$ and $E_{r0} = eK^*/(ir)^{E-D-1}$.

Those equations can be then used for example to study the transport of the heat through the matter. The specific yield of the heat source $q_0(r)$ as described in (3.1) is then used.

$$q_0(r) = eKr^{D-E}, \quad (8.4)$$

We can determine density of heat flow rate $\mathbf{q}(r)$ (in $\text{J.m}^{-2}.\text{s}^{-1}$) and temperature $T(r)$ ($q_0 = \text{div } \mathbf{q} = \text{div}(-\lambda \text{grad } T) = -\lambda \Delta T$), where λ is constant thermal conductivity (in $\text{J.m}^{-1}.\text{s}^{-1}.\text{K}^{-1}$). For radial temperature field we can write

$$q_r = eK \cdot \frac{r^{D-E+1}}{D}, \quad T_r = -\frac{eK}{\lambda} \cdot \frac{r^{D-E+2}}{D(D-E+2)}. \quad (8.5)$$

If we suppose that heat parameters through the surrounding by the constant diffusivity in time $r^2 = 4a_0t - r_T^2$, where $r_T^2 = x^2 + y^2 + z^2$ is the radius of fractal space and a_0 is the maximum value of diffusivity (for $D = E$), we get from (8.5)

$$T_r = -\frac{eK(4a_0t)^{(D-E+2)/2}}{\lambda D(D-E+2)} \left(1 - \frac{r_T^2}{4a_0t} \right)^{(D-E+2)/2}. \quad (8.6)$$

If the heat diffuses by the significantly lesser speed ($r_T^2 \ll a_0t$, small distances or long times) the terms in parenthesis can be observed as significant in the expansion of exponential function ($1 - x \approx e^{-x}$) and we can write then

$$T_r = -\frac{eK(4a_0t)^{(D-E+2)/2}}{\lambda D(D-E+2)} \exp\left(-\frac{D-E+2}{2} \cdot \frac{r_T^2}{4a_0t} \right). \quad (8.7)$$

If we substitute for the thermal conductivity $\lambda = c_p \rho a = 2c_p \rho a_0 / (D - E + 2)$, where c_p is specific heat capacity after constant pressure (in $\text{J.kg}^{-1} \cdot \text{K}^{-1}$), ρ mass density (in kg.m^{-3}) and a the coefficient of thermal diffusivity of the body with fractal dimension D (in $\text{m}^2 \cdot \text{s}^{-1}$) we obtain

$$T_r = -\frac{2eKt}{c_p \rho D} [2at(D - E + 2)]^{(D-E)/2} \exp\left(-\frac{r_T^2}{4at}\right) \quad (8.8)$$

For the total heat transferred to the body from the heat source $Q = -2eKt/D[(D - E + 2)/2\pi]^{(D-E)/2}$ we obtain

$$T_r = \frac{Q}{c_p \rho (4\pi at)^{(E-D)/2}} \cdot \exp\left(-\frac{r_T^2}{4at}\right) \quad (8.9)$$

The relation (8.9) is applicable for fractal dimensions $D = 0, 1, 2$ and topological dimension $E = 3$, see *Figure 20*.

The maximum position can be determined by the derivation of (8.9) with the time

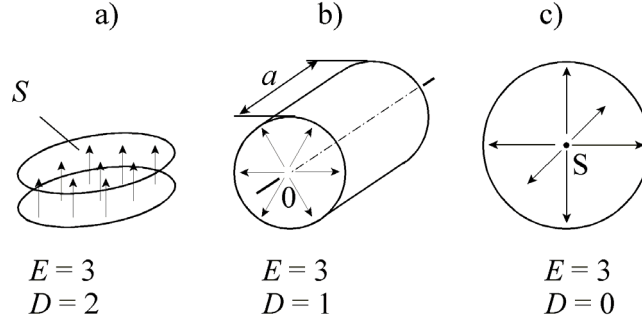


Figure 20 Heat flow geometry for a) plane-parallel, b) cylindrical and c) spherical coordinates Euclidean space.

$$\frac{\partial \log T}{\partial \log t} = \left(\frac{D - E}{2} + \frac{h^2}{4at} \right) = 0 \quad (8.10)$$

From this equation the thermal diffusivity at the maximal time can be determined

$$a = \frac{h^2}{2t_m f_a} = \frac{h^2}{2(E - D)t_m} \quad (8.11)$$

where f_a is a coefficient that characterizes the deformation of the thermal field (8.4). This coefficient is equal to one for the ideal plane source ($E = 3, D = 2$). The maximum temperature of the response for Dirac thermal pulse is obtained by introducing of the thermal diffusivity (8.11) in the term (8.9)

$$T_m = \frac{Q}{c_p \rho} \exp\left(\frac{D - E}{2}\right) \cdot \left(\frac{E - D}{2\pi h^2}\right)^{(E-D)/2} \quad (8.12)$$

From the ratio of Eq. (8.12) and (8.9) and with the use of the term (8.11)

$$\frac{T_m}{T} = \left[\frac{t}{t_m} \exp\left(\frac{t_m}{t} - 1\right) \right]^{\frac{E-D}{2}}, \quad \frac{T_m}{T} = \left[\frac{t}{t_m} \exp\left(\frac{t}{t_m} - 1\right) \right]^{\frac{E-D}{2}} \quad \text{respectively,} \quad (8.13)$$

it is possible to define the coefficient f_a (fractal dimension D respectively) for every point of the experimental dependence

$$f_a = E - D = \frac{2 \ln(T_m/T)}{\ln(t/t_m) + (t_m/t - 1)}, \quad f_a = E - D = \frac{2 \ln(T_m/T)}{\ln(t/t_m) + (t/t_m - 1)}, \quad (8.14)$$

respectively.

The relations on the left side are used for the temperature increase; the relations on the right side are used for the temperature decrease. The value of the coefficient f_a could be also affected by the geometry of sample or by the finite pulse width, too.

From term (8.12) the thermal capacity is obtained

$$c_p = \frac{Q}{\rho T_m h_T} \cdot \frac{f_c}{\sqrt{2\pi \exp(1)}} = \frac{Q}{\rho T_m h^{E-D}} \cdot \left(\frac{E-D}{2\pi \exp(1)} \right)^{(E-D)/2} \quad (8.15)$$

and thermal conductivity of the studied fractal structure

$$\lambda = c_p \rho a = \frac{Q}{2(E-D)T_m t_m h^{E-D-2}} \cdot \left(\frac{E-D}{2\pi \exp(1)} \right)^{(E-D)/2}, \quad (8.16)$$

where f_a and f_c are the coefficients that characterize the deformation of the thermal field.

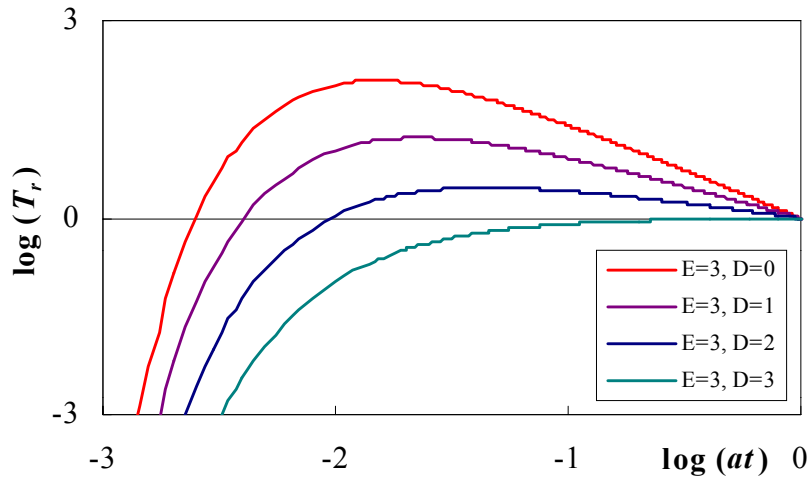


Figure 21 Time dependency of the temperature response for the Dirac thermal pulse (for the heat flow geometry from Figure 20 calculated by Eq. (8.9))

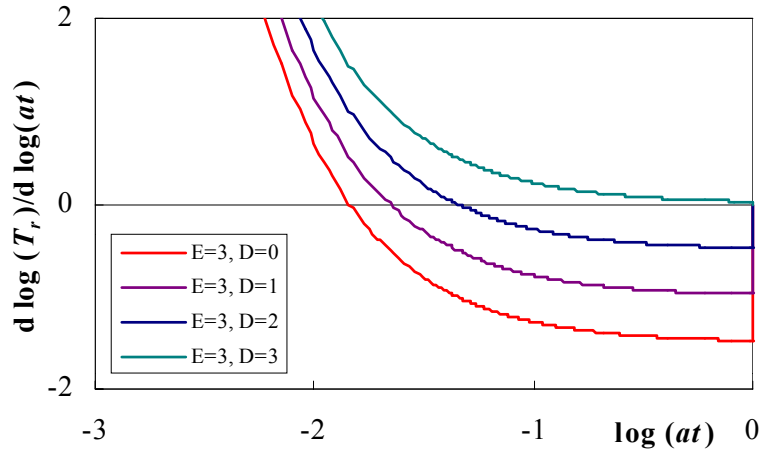


Figure 22 Time dependency of the slope temperature response for the Dirac thermal pulse (for the heat flow geometry from Figure 21 calculated by Eq. (8.10)).

The Figure 21 represents time-temperature dependencies (according to Eq. (8.9)) calculated for spherical ($D = 0$), cylindrical ($D = 1$), planar ($D = 2$), and cubic ($D = 3$) geometry of the heat source (see Figure 20). It is evident from the Figure 21 and from the Eq. (8.10) that for $D = E$ the function meets maximum for the time $t \rightarrow \infty$.

All dependences for the long time intervals converge to the asymptote, which is longitudinal with the time scale. The intersection of this asymptote with the vertical scale determines the coefficient $f_a = (E - D)$ and thus the fractal dimension D that characterizes the specimen set-up (heat source, specimen, distribution of the temperature field, heat losses). When the value f_a is known it is feasible to determine the parameters of the studied thermal system with the aid of the Eq.(8.11) – (8.16).

The Thermophysical Transient Tester 1.02 we use for measuring of the responses to the pulse heat. It was developed at the Institute of Physics, Slovak Academy of Science.

Thermal responses from Slovak Academy were used for the data evaluation. The measured sample was round shaped with diameter $R = 0.03$ m. Its density was $\rho = 77.9 \text{ kg.m}^{-3}$ for its thickness $h = 0.0075$ mm, the thermal conductivity was $\lambda = 0.0254 \text{ W.m}^{-2}.\text{K}^{-1}$.

In Figure 23 three possible configurations of experiment arrangements are shown. In Figure 23a the diameter of specimen is equal to the diameter of a heat source, in Figure 23c diameter of a heat source is far smaller than specimen's diameter. Figure 23b shows the real situation, when the heat is delivered irregularly (either from the source of finite size (capacity) or from a source with specific composition of heat sources – e.g. hot-disc).

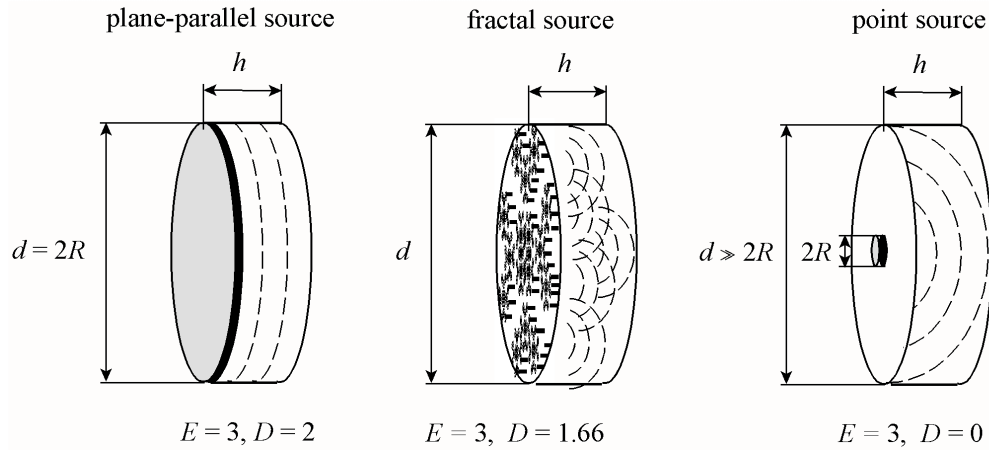


Figure 23 Current flow geometry: a) plane-parallel, b) fractal, c) point (for different ratio of length contact respectively) source.

The Figure 24 represents the typical time responses of temperature for the step wise of input power. The coefficient f_a (fractal dimension D respectively) of the fractal heat source for every point of the experimental dependence (measured dependency of temperature on time) was calculated using the Eq. (8.14). The fractal heat source characterizes the distribution of the temperature in the specimen in specific time. From the Figure 25 it is evident that for very short time fractal dimension gains $D \approx 2$, and therefore, the plane heat source is formed. The value of the fractal dimension decreases with increasing time, since the heat disperses into the space. From the time $\tau_1 \approx 16$ s (the intersection of tangents of the curves) the fractal dimension is getting settled to the value $D \approx 0.15$. The spatial distribution of the temperature in the sample does not change yet in this area. It is possible to determine the coefficient of the heat source $f_{a0} = 1$ and the diffusivity of the specimen $a \approx 4.679 \cdot 10^{-7} \text{ m}^2 \text{ s}^{-1}$ from the extrapolated curve of the fractal dimension to the time $t = 0$ s. This value is identical to findings determined by the Institute of Physic, Slovak Academy of Sciences, Bratislava.

The deviations between the experimental (the black curve) and the model (the red curve) response obvious in the descending part of the characteristics are caused by the heat dissipation from the material via the cylinder surface of the specimen. This causes a faster decrease of the temperature than the theory predicted. The course of the temperature deviation between the model and experimental characteristic are illustrated as the blue curve in the Figure 24. Negative values of functional dependence show the heat dissipations from the specimen. This deviation has also its own extreme (minimum), which means that for the value of time $t_m < 250$ s heat losses are rising and for longer time intervals heat losses are smaller.

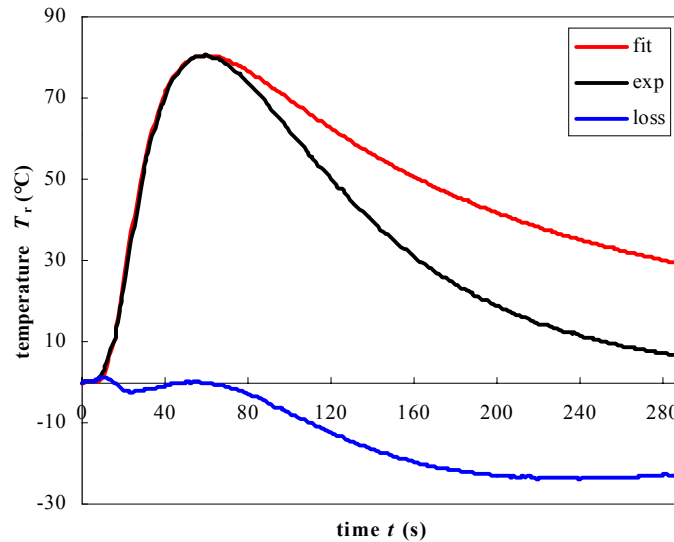


Figure 24 Thermal response of the sample measured by the pulse transient method (black – experimental data, red – model data, blue – difference between experimental and model data).

From the descending characteristic we can again determine, by using (8.14) for each point of experimental dependence of measured temperature on time, coefficient f_a , fractal dimension D of the fractal source “of cold” presented by specimen surface. From Figure 25b it is evident that there are not any cold spots over the surface of specimen for time intervals close to the maximum (the fractal dimension of heat spots is equal to the topological dimension $D \approx 3$. With rising time the value of fractal dimension of decreasing temperature is smaller until the value $D \approx 2$. This is a fractal dimension of the specimen surface. The time constant of this descent is $\tau_2 \approx 86$ s. From the proportion of time constants (expecting that diffusivity of the

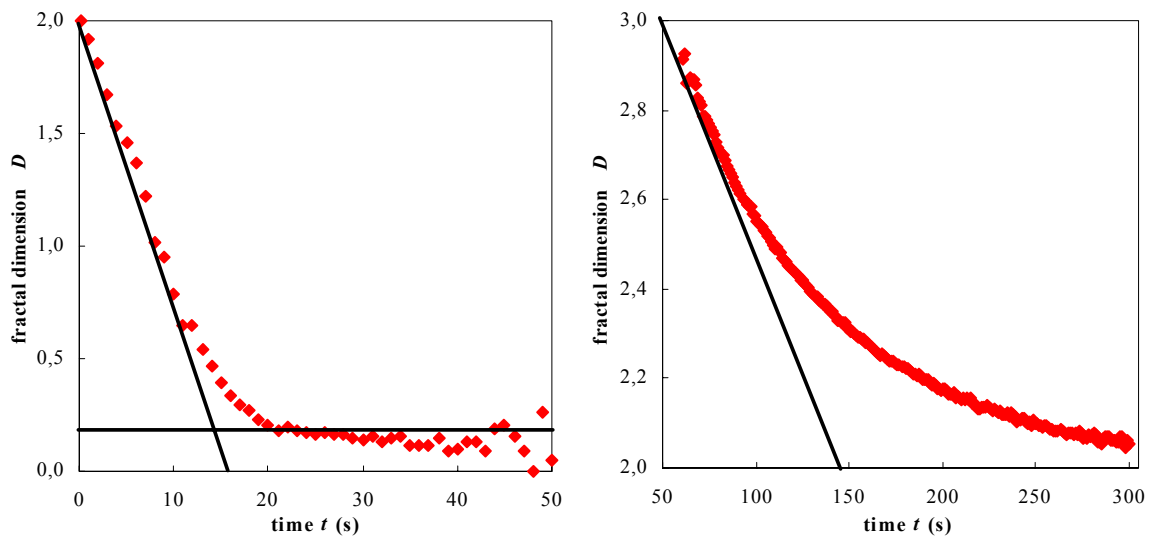


Figure 25 Fractal dimension of the heat distribution in the specimen from a) increased and from b) decreased part of characteristics.

material does not change) we can presume the distance between the source of heat dissipation and the thermocouple $x = h\sqrt{\tau_2/\tau_1} \approx 0.017\text{m}$. This value approximately responds to the specimens' radius.

9. CONCLUSION

The possibilities of the use of the fractal geometry for description of different physical effects were discussed. Obtained information can lead to the new view on different kinds of static and dynamic physical fields (e.g. gravitational, electrostatical, electrodynamical, and thermal) and can also help when studying properties of elementary particles.

10. REFERENCES

- [1] Mandelbrot B. B.: Fractal Geometry of Nature, W.H. Freeman and Co., New York, (1983).
- [2] Barnsley MF. Fractals Everywhere. Boston: Academic Press; 1988
- [3] Theiler J. Estimating fractal dimension. J. Opt. Soc. Am. A 19; 6(7): 1055–1073
- [4] Zmeskal O, Nezadal M, Buchniecek M. Fractal–Cantorian Geometry, Hausdorff Dimension and the Fundamental Laws of Physics. Chaos, Solitons & Fractals 2003; 17: 113–119
- [5] Zmeskal O, Nezadal M, Buchniecek M. Field and potential of fractal–Cantorian structures and El Naschie's $\varepsilon(\infty)$ theory. Chaos, Solitons & Fractals 2004; 19: 1013–1022
- [6] Zmeskal O, Buchniecek M, Bednar P. Coupling constants in fractal and cantorion physics. Chaos, Solitons & Fractals 2004; 19: 1013–1022
- [7] Zmeskal O., Buchniecek M., Vala M.: Thermal Properties of bodies in fractal and cantorion physics, Chaos, Solitons & Fractals 25:, 941–954, (2005)
- [8] Raby S. Grand Unified Theories. The Review of Particle Physics 2002; Editor: Hagiwara K. et al., D66: 010001-1, <http://www-pdg.lbl.gov/>
- [9] Lloyd S. Elementary Particle Physics. Editor Lloyd S., Queen Mary University of London. <http://hepwww.ph.qmul.ac.uk/epp/>
- [10] Goldfain E. Derivation of lepton masses from the chaotic regime of the linear σ – model. Chaos, Solitons & Fractals; 2002; 14: 1331–1340
- [11] Marek-Crnjac L. On the mass spectrum of the elementary particles of the standard model using El Naschie's golden field theory. Chaos, Solitons & Fractals; 2003; 15: 611–618
- [12] El Naschie MS. On a class of general theories for high-energy particle physics. Chaos, Solitons & Fractals 2002; 14: 649–668

- [13] Goldfain E. Derivation of lepton masses from the chaotic regime of the linear σ – model. *Chaos, Solitons & Fractals*; 2002; 14: 1331–1340
- [14] El Naschie MS. On the exact mass spectrum of quarks. *Chaos, Solitons & Fractals*; 2002; 14: 369–376
- [15] Hagiwara K. et al. (Particle Data Group), *Phys. Rev. D* 66, 010001 (2002) (<http://pdg.lbl.gov/>)
- [16] El Naschie MS. Quantum gravity, Clifford algebras and the fundamental constants of nature. *Chaos, Solitons & Fractals*; 2004; 20: 437–450
- [17] El Naschie MS. A review of E infinity theory and the mass spectrum of high energy particle physics. *Chaos, Solitons & Fractals*; 2004; 19: 209–236
- [18] Stöckmann F. An Exact Evaluation of Steady-State Space-Charge Limited Currents for Arbitrary Trap Distribution, *Phys. Stat. Sol.* 1981; A64: 475-483
- [19] Zmeskal O., Schauer F., Nespurek S. The Bulk Trap Spectroscopy of Solids by Temperature Modulated Space-Charge-Limited Currents (TMSCLC) in the Steady State. 1985; 18: 1873-1884
- [20] Schauer F., Nespurek S., Zmeskal O. The Bulk Trap Spectroscopy of Solids by Temperature Modulated Space-Charge-Limited Currents (TMSCLC): Application to Real Crystalline and Amorphous Semiconductors. 1986; 19: 7231-7246
- [21] Lampert M. A., Mark P.: *Current Injection in Solids*, Academic Press, New York and London, 1970
- [22] Carslaw HS, Jaeger JC. *Conduction of Heat in Solids*. Oxford University Press, 2003
- [23] Atkins PW. *Physical Chemistry*. Oxford University Press, 1998
- [24] Halliday D, Resnick R, Walker J. *Fundamental of Physics*. John Wiley & Sons, 2001